The Strait of Messina: Seismotectonics and the source of the 1908 earthquake

G. Barreca[1,2*], F. Gross[3,5], L. Scarfì[4], M. Aloisi[4], C. Monaco [1,2,4], S. Krastel[3]

1) Dipartimento di Scienze Biologiche Geologiche e Ambientali, Università di Catania

2) CRUST - Interuniversity Center for 3D Seismotectonics with territorial applications.

3) Center for Ocean and Society, Kiel University, Kiel, Germany

4) INGV – Osservatorio Etneo, Catania

5) Institute of Geosciences, Kiel University, Kiel, Germany

Corresponding Author

g.barreca@unict.it

Giovanni Barreca

Address:

Corso Italia 57, 95129 Catania, Italy

Abstract

More than 100 years after the devasting Messina-Reggio Calabria earthquake (M=7.1), the largest seismic event ever recorded in southern Europe in the instrumental epoch, its causative seismic source is still unknown, and the several rupture models proposed in the last decades are far from any shared solution. Data interpretation on a new dataset of sub-seafloor geophysical soundings with unprecedented resolution, relocated seismicity, and V_p model, together with morphotectonic investigations and inverse modelling of available levelling data, provide additional constraints on the deformation mechanisms and seismotectonics of the Strait of Messina area. High-resolution seismic lines in the offshore, along with displaced Quaternary marine terraces on land, point to active deformation along a previously unmapped ~ 34.5 km-long extensional fault. Spatial distribution of relocated earthquakes highlighted that a cut-off of the seismicity occurs within the crustal depth. The seismic discontinuity roughly delineates a foreland-dipping and low-angle discontinuity apparently confirming previous studies predicting low-angle seismogenic sources for the 1908 seismic event. However, according to the overburden stress and the attitude of the discontinuity, stress analysis suggests that a seismic slip is unlikely along it. This therefore weakens the hypothesis that a large earthquake may have nucleated along the low-angle discontinuity. Rather, aseismic creeping is instead expected since movement is allowed only by assuming a mechanical weakness of the plane. This mechanical behaviour is currently also supported by the large interseismic strain-rate recorded in the area. Both seismic tomography and crustal-to-subcrustal scale 3D-modelling strongly suggest a cause-and-effect relationship between slab retreat, mantle wedging, uplift in the upper plate block, and active extension in the Strait of Messina area. Lithospheric doming of the upper plate is here interpreted to be the main process controlling uplift in the Peloritani Mts. of Sicily and subsidence in the Strait of Messina region where deformation is mainly accommodated by the weak low-angle discontinuity. In this frame, an almost aseismical slip toward the foreland of the low-angle discontinuity is here interpreted to produce stress perturbation in the area. Coulomb stress change modelling revealed that simulated normal slip on the foreland-dipping discontinuity can induce additional stress and promote failure in the overlying brittle faults. An excellent fit between calculated and observed subsidence is achieved by geodetic data inversion that resolved a normal slip on the low-angle discontinuity and a transtensional (slightly left-lateral) motion on the 34.5 km-long and previously unknown extensional fault. The fault-length along with the observed seafloor displacement make this tectonic structure as the most likely to have produced large earthquakes in the Strait of Messina area.

Keywords: Messina-Reggio Calabria earthquake, seismic reflection data, causative fault, seismicity cut-off, stress transfer, 3D modelling

1. Introduction

The Strait of Messina in southern Italy is a roughly NS trending, ~3 km wide seaway separating the Italian peninsula from the island of Sicily. The Strait of Messina is considered a highly hazardous area from a seismic viewpoint since it was struck by one of the most powerful seismic events (M 7.1) ever recorded in the Italian peninsula in the instrumental epoch. The disastrous event occurred in the early morning of 28th December 1908 and was accompanied by a tsunami, which inundated the Calabrian and Sicilian coastlines a few minutes after the initial seismic event (Platania, 1909). The

74 severe ground shaking and tsunami impact on the coasts were responsible for more than 100.000
75 deaths (Mercalli, 1909; Omori 1909), making the Messina-Reggio Calabria earthquake the deadliest
76 event in Europe. The earthquake was felt all over southern Italy and towards the south on the Maltese
77 islands, with major damages (X-XI EMS, see Barbano et al., 2005) concentrated over a ~ 4000 km^2
78 box-shaped region encompassing the Strait of Messina. A higher degree of damage was reported in
79 Calabria than in Sicily (Baratta, 1910; Mulargia and Boschi, 1983). Since this devasting event, several
80 studies have attempted to define the active deformation field governing the area along with the
81 location, geometry, and kinematics of the 1908 causative seismogenic fault. Inverse modelling of
82 seismograms (Boschi et al., 1989; Bottari et al., 1989) and available geodetic levelling data, measured
83 before and after the mainshock (Loperfido, 1909), have for a long time been used as input data to
84 propose extensional rupture as well as many and often debated fault source models. Indeed, modelled
85 causative faults span from blind low-angle E-dipping (Sicilian side, see Capuano et al., 1988; Boschi
86 et al., 1989; De Natale and Pingue, 1991; Valensise and Pantosti,1992) to outcropping W-dipping
87 high-angle (Calabrian side, see Mulargia and Boschi, 1983; Bottari, et al., 1989; Shick, 1997; Aloisi
88 et al., 2012) extensional faults. Although there is a consensus on the deformation affecting the
89 mainland sectors of the Strait of Messina, the offshore tectonic setting, where the 1908 epicentre was
90 located (Schick,1977), has remained poorly understood and constrained. To a large extent, this lack
91 of a thorough understanding reflects the unavailability of marine geophysical data with a suitable
92 resolution. The offshore sector of the Straits was first highlighted by Argnani (2009) throughout a
93 grid of multichannel seismic profiles. However, the low-medium resolution of the seismic dataset
94 only allowed providing a general overview of the seismo-stratigraphic architecture of the Straits,
95 whereas the tectonic pattern remained unimaged and hence unresolved. More recently, interpretation
96 over a new seismic reflection dataset described the Strait of Messina and surrounding areas as a
97 complex tectonic puzzle where active transpressional and transtensional deformation, arising from
98 independent and overlapping tectonic processes, take place simultaneously (Doglioni et al., 2012).
99 High-resolution seafloor mapping (Ridente et al., 2014) shed light on the morpho-bathymetric

features occurring in the submerged area of the Strait. According to seafloor mapping, the most prominent morpho-structural feature is the axial channel of the Messina Canyon (Colantoni, 1987), a near-rectilinear NNE-SSW trending submarine incision. This incision is characterized by a steeper western flank at which several geomorphic features such as triangular facets and suspended incisions indicate recent/active deformation, even if evidence of seafloor ruptures was not reported by the authors alongside the submarine incision. Several submarine landslides were instead identified and mapped along the eastern slope of the Straits on the Calabrian side.

Despite several remarkable papers published over the last decades concerning primarily the identification of the seismogenic source of the 1908 event, the lack of coseismic ruptures both on-land (Baratta, 1910) and offshore along with the unavailability of suitable sub-seafloor geophysical soundings, make this issue far from solved. Apart from this, several other open questions, which are essential to understand the seismotectonic regime of the Strait of Messina region, have remained elusive. For instance, the geodynamic process from which tectonic stretching originated in the area is still controversial, ranging from subduction cessation and plate reorganization (Goes et al., 2004), rapid slab retreating and asthenosphere suction (Gvirtzman and Nur, 1999), and tectonic collapse following the eastward retreating of the Ionian plate (Doglioni et al. 1999). Given the lack of suitable information on the subcrustal setting beneath the Strait of Messina, the possible kinematic links between deep-seated geodynamics and near-surface processes have not been thoroughly explored. Through a cross-disciplinary investigation, including high-resolution marine geophysical data interpretation, geomorphological analysis, high-precision relocated seismicity, and tomographic models, we critically reviewed most of the literature regarding the deformation pattern and seismotectonics of the Strait of Messina area. The interpretation of a dense grid of multichannel seismic lines with unprecedented resolution, revealed in detail the sub-seafloor tectono-stratigraphic setting of the Strait of Messina, providing original constraints on both the through-time geological evolution and on the recent/active deformation field including the long-searched evidence for surface faulting in the area. Spatial distribution of relocated earthquakes highlights how seismic stress is

126 dissipated in the crust and leads to image previously undetected seismicity cut-off beneath the Strait
127 of Messina. Such cut-off, which seems to delineate a large crustal discontinuity dipping at a low-
128 angle towards the Ionian foreland, has been considered here as having a significant role in the
129 seismotectonic of the area. V_p models allow achieving suitable information on the Africa-Europe
130 plate boundary dynamic at the subduction zone. The comprehensive interpretation in the 3D
131 environment of the newly provided data, along with rock mechanics analysis, numerical simulation,
132 and a different point of view on the historical observations and measurements available for the 1908
133 earthquake, allow supporting an alternative deformation model for the Strait of Messina region in
134 which seismic and aseismic processes can interact with each other to produce large earthquakes in
135 the area. The proposed deformation model, together with novel surface evidence for faulting in the
136 area and 3D reconstruction of the subcrustal setting, finally concurred to question most of the
137 previously inferred causative faults and seismic sources modelled for the 1908 Messina-Reggio
138 Calabria earthquake and to confirm some points about the deeper geodynamic processes and their
139 kinematic relationships with the shallowest Quaternary deformation in the area.
140
141 ## 2. Background
142
143 The Strait of Messina, in the central Mediterranean region (Fig.1A), is a narrow sea-channel lying in
144 the fore-arc region of the Ionian subduction zone (Fig. 1B). The Straits is an NNE-SSW trending,
145 sigmoidal-shaped structural depression, about 40 km-long and with variable width spanning from 3
146 km in the north to 16 km in the south. It opened since the middle Pleistocene (Monaco et al.1996)
147 owing to crustal extension dynamics involving the inner-southernmost sector of the Calabrian Arc
148 (Fig. 1A). Extensional tectonics in the area has been explained through several large-scale processes,
149 mostly connected to the rolling-back dynamics of the Ionia slab at depth (Doglioni et al., 1999;
150 Gvirtzman and Nur, 1999). The investigated sector falls above the hinge zone of the Ionian subduction
151 system (Fig. 1C), a long-lived geodynamic process developed in the frame of the Africa-Europe plate
152 convergence because of the sinking of the Ionian oceanic lithosphere (African margin) beneath the

153 European block (Malinverno and Ryan, 1986; Jolivet and Faccenna, 2000; Faccenna et al., 2001).
154 Since ~35 Ma, the rapid SE-wards rolling-back of the Ionian slab controlled the tectonic evolution of
155 the Western Mediterranean region with the opening of large back-arc extensional basins (i.e. the
156 Ligurian-Provençal and Tyrrhenian Basins, see Scandone, 1979; Malinverno and Ryan, 1986; Patacca
157 and Scandone, 1989; Faccenna et al., 2004). Back-arc opening was accompanied by trench migration
158 and the consequent accretion ahead of narrow, foreland-verging orogenic wedges (see Faccenna et
159 al., 2014 and references therein). The time-progressive shortening was lastly responsible for the
160 shaping of the Apennine-Maghrebian Chain, a large orogenic domain extending from the Maghrebian
161 region in NE Africa to the Apennines in Italy, across the Calabrian Arc. The Calabrian Arc (CA in
162 Fig. 1A, see Amodio Morelli et al, 1976), originated from the deformation of the European paleo-
163 margin. The CA occupies currently the highest structural position in the orogenic system being over-
164 thrusted over the laterally variable (continental to oceanic) African block. It consists of an arched-
165 shaped terrane (Johnston and Mazzoli, 2009) formed by a pile of tectonic slices resulting from the
166 imbrication of European-derived rocks consisting mainly of Hercynian metamorphic basement and
167 remnants of Meso-Caenozoic carbonate covers (Ogniben, 1969). The CA and its continental root
168 form the upper plate region of the subduction zone currently with the role of backstop in the
169 collisional system. The SE-wards migration of the European backstop has been responsible for the
170 growth of a large accretionary prism in the Ionian Sea (Fig. 1 B) where sediments, scraped from the
171 descending slab, progressively emplaced. Although the Calabrian Arc lies in the fore-arc region of
172 the subduction system where shortening is usually expected, the late Quaternary deformation field is
173 that of an extending domain with large normal faults running along its axial zone (Fig. 1B).
174 Extensional faulting overprinted previous compressional features in the area (Monaco et al., 1996)
175 and was produced by crustal extension along the WNW-ESE-trending direction (Tortorici et al., 1995;
176 Monaco and Tortorici, 2000; Jacques et al., 2001). Fault activity was accompanied by a significant
177 vertical uplift with the formation of footwall-highs and fault-bounded marine basins including the
178 Strait of Messina structural depression (Ghisetti and Vezzani, 1982; Ghisetti, 1984; Monaco and

179 Tortorici, 2000). Being the CA located atop the slab hinge (see Fig. 1C), regional uplift and extension
180 in the region have been commonly related to deep-seated asthenosphere processes or to plate
181 reorganization connected to the stalling of slab retreating process (e.g. Westaway, 1993; Wortel and
182 Spakman, 2000; Doglioni et al., 2001; Gvirtzman and Nur, 1999; Goes et al., 2004). Several studies
183 interpreted the fault-bounded Strait of Messina depression as the southern termination of a larger
184 extensional belt running longitudinally across the Calabrian mainland (Ghisetti and Vezzani, 1982;
185 Ghisetti, 1984). The belt includes several other normal faults such as the Cittanova, Scilla, S. Eufemia,
186 Reggio Calabria and Armo faults (see Westaway, 1993; Jacques et al., 2001; Ferranti et al., 2007;
187 Tortorici et al. 1995 and Fig. 1D for location), characterized by a late Quaternary activity and to
188 which strong historical seismicity has been associated (e.g. the 1783 and 1908 events, see CPTI15
189 and Rovida et al., 2016). New seismological data from the Calabrian Arc (Sgroi et al., 2021), suggest
190 the Messina Strait as an arc-orthogonal extensional depression kinematically linked to the
191 propagation of a larger NW-SE dextral shear zone (Polonia et al., 2011, 2016; Barreca et al., 2019)
192 bounding the Strait to the south. Whatever the geodynamic process producing deformation in the
193 area, crustal extension along the Calabrian Arc persists to the present-day as documented by the
194 normal solutions of earthquakes with M>5.5 occurring in the area (Gasparini et al., 1981; Dziewonski
195 et al., 1987; Pondrelli, 2002, see Fig. 1 B for earthquake location) and the measured differential
196 geodetic velocities (D'Agostino and Selvaggi, 2004; Mattia et al., 2009; Serpelloni et al., 2010;
197 D'Agostino et al., 2011, see blue arrows in Fig. 1D).
198
199 *2.1 Geology of the Strait of Messina*
200
201 As evidenced by several tectono-stratigraphic studies performed on-land (Tortorici et al. 1995;
202 Monaco et al., 1996; Monaco and Tortorici 2000; Di Stefano and Longhitano, 2009, Lentini et al.,
203 2000), the opening of the Strait of Messina area can be dated back to 0.8 - 0.6 Ma. Extensive field
204 mapping (Lentini et al., 2000 and reference therein) along with observed unconformities separating

205 the various stratigraphic units (Monaco et al., 1996), identify the Strait of Messina as an extensional
206 Pleistocene syn-tectonic basin filled by marine to continental deposits. Top-set basin closure
207 succession consists of a huge volume of middle Pleistocene Gilbert fan delta-type deposits (Barrier,
208 1987), locally known as the Messina Gravels and Sands Fm. and widely outcropping on both sides
209 of the Straits. The Messina gravels show occasionally conglomeratic facies at the bottom and lie
210 unconformably atop the middle Pleistocene clays and calcarenites of the Spadafora and S. Corrado
211 formations, respectively. Older deposits consist of Upper Miocene-Pliocene rock series which include
212 Tortonian conglomerates, Messinian evaporites, and Lower Pliocene whitish globigerina-bearing
213 marly limestones (Trubi Fm., see Servizio Geologico d'Italia, 2007 for an overview). From the
214 structural point of view, the Strait of Messina is a rather tectonically unstable area where intense
215 Quaternary activity is evident due to the occurrence of raised marine terraces, which can be observed
216 widespread on both sides of the Straits (Monaco et al., 2017 and reference therein). The estimated
217 uplift of over 2 mm per year is among the fastest documented in Italy and has been associated to
218 combined, regional long-term, and local fault-related short-term signals (Westaway, 1993; Antonioli
219 et al., 2006; Ferranti et al., 2007; Monaco et al., 2017 and reference therein). The local contribution
220 is attributed to the late Quaternary activity of the extensional fault belt deforming the eastern and
221 western mainland sectors of the Strait of Messina (Fig.1 D). Surface evidence for faulting is more
222 prominent at the Calabrian side, where several NE-SW trending structures (i.e. the Armo, Reggio
223 Calabria and Scilla faults, see Fig. 1D for location) appear to have slipped recently, as suggested by
224 field (Ghisetti and Vezzani, 1982; Ghisetti, 1981;1984; Tortorici et al., 1995; Aloisi et al., 2012) and
225 coastal tectonic studies (Ferranti et al., 2007; Scicchitano et al., 2011). Conversely, evidence for
226 recent faulting in the Sicilian side remains doubtful, since deformation along few and scattered fault
227 segments, appear not to have involved sediments younger than the middle Pleistocene. Considerable
228 uncertainties also remain concerning the continuation of such bounding faults in the offshore realm.
229 The only known exception are the northernmost and narrower sectors of the Straits, where recent
230 faulting has been evidenced by high-resolution swath bathymetry and multichannel sparker profiles

231 (i.e. along the Scilla Fault, see Ferranti et al., 2008 and Fig. 1 C for location). Less sophisticated
232 bathymetric and geophysical data were used by previous authors (Del Ben et al., 1996; Argnani et al.,
233 2009) to infer the occurrence of active faults on the eastern (Calabrian) side of the Straits. GPS
234 velocity measurements and fault investigations suggest that the Straits is opening at a rate of 1.5 - 3.4
235 mm/a in the WNW-ESE to NW-SE direction (D'Agostino and Selvaggi, 2004; Ferranti et al. 2007)
236 and subsiding at 1 mm/a (Bottari et al. 1989; De Natale and Pingue 1991; Amoruso et al. 2002).
237
238 *2.2 Previous models on the 1908 causative fault and their weaknesses*
239 Available seismograms registered by 110 globally distributed seismic stations were exploited over
240 the past decades by several authors to propose a rupture mechanism for the 1908 earthquake (Schick,
241 1977; Caputo, 1979; Gasparini et al., 1982; Mulargia and Boschi, 1983; Bottari et al., 1986; Boschi
242 et al., 1989; De Natale and Pingue, 1991; Pino et al., 2000; Amoruso et al., 2002; Michelini et al.,
243 2005, see also Pino et al., 2009 for an overview). Besides the proposed faulting mechanisms differing
244 slightly from each other regarding fault parameters (i.e. strike, dip, and length of the fault), there is
245 consensus about an extensional rupture that occurred on a NNE-SSW trending plane. On the contrary,
246 inversion of the levelling data and of the macroseismic field (Loperfido, 1909; Baratta, 1910;
247 Mulargia and Boschi, 1893, see Fig. 2 A and B respectively) leads to several, often contrasting,
248 models of the 1908 causative fault (Fig. 2C). Indeed, the models range from two opposite-dipping
249 normal faults with different dip-angle (Mulargia and Boschi, 1983; Aloisi et al., 2012) to E-dipping
250 blind low-angle fault on the Sicilian side (Capuano et al., 1988; De Natale and Pingue, 1991; Boschi
251 et al., 1989; Valensise and Pantosti, 1992; Amoruso et al., 2002) or to W-dipping high-angle fault
252 ruptured on the Calabrian mainland (Aloisi et al., 2012) or right along the Straits (Shick, 1997).
253 Macroseismic field along with structural and morphotectonic investigations have instead been used
254 by other authors to infer rupture along the NE trending, west-dipping faults slicing across the
255 Calabrian side of the Strait (Bottari et al., 1986; Ghisetti, 1984; 1992; Westaway, 1992; Tortorici et
256 al., 1995; Bottari, 2008). This hypothesis was supported, in addition to field data, by the highest

257 degree of damage in southern Calabria (Fig. 2D) where significant subsidence and coseismic ground
258 fracturing were also recorded (Monaco and Tortorici, 2007; Blumetti et al., 2008). An enhanced uplift
259 of the out-of-water marine terraces in southern Calabria, which is higher than on the Sicilian side of
260 the Straits (Ferranti et al., 2007; Monaco et al., 2017 and reference therein), could in fact be in favour
261 of a seismotectonic scenario dominated by an activity along the W-dipping normal faults. Using
262 additional information such as seismicity and morphotectonic data, Aloisi et al. (2012) speculated
263 that the Armo and the S. Eufemia faults were part of a major crustal structure that slipped during the
264 1908 earthquake. A recently published work (Meschis et al., 2019) proposes a rupture along the so-
265 called Messina-Taormina Fault (MTF in Fig. 1D), a 70 km-long structure running close to the Sicilian
266 coast. Analogue modelling reproducing the structural architecture of the Strait (Bonini et al., 2011)
267 suggested that high-angle and low-angle normal faults could coexist in the same tectonic framework.
268 The model predicted that slip on a low-angle and E-dipping master fault could be accompanied by a
269 crestal graben formation and secondary antithetic W-dipping structures in the hanging-wall block.
270 However, the adopted angle of internal friction of 24° for the material reproducing a low-angle fault
271 core is not in favour of a coseismic slip along this structure (see section 6). In the absence of evidence
272 for surface faulting, the 1909 re-levelling measurements have for a long time represented the only
273 input data for source modelling. However, the lack of information on possible surface deformation
274 preceding the 1908 mainshock weakens the assumption that measured subsidence must necessarily
275 represent a coseismic deformation. More precisely, what is known is only that vertical deformation
276 was achieved after the 1908 mainshock (Loperfido, 1909) by the difference with pre-earthquake
277 measurements. However, pre-earthquake measurements do not necessarily mark the onset of
278 subsidence in the area. Accordingly, if and how long time before the earthquake the subsidence
279 process started is unknown and it could already have been underway before the 1908 mainshock.
280 Further, a long-ignored issue is that negligible or no uplift was registered by levelling measurements
281 at the borders of the box-shaped subsiding area. The Peloritani Mts. in Sicily, namely the footwall
282 block for several models predicting E-dipping faults, remained stable or slightly subsided right where

uplift was instead expected (see Fig. 2B). This aspect raises some questions about the deformation from which subsidence generated, pointing towards a possible occurrence of gravity-driven processes equally capable of generating the observed surface deformation (see section 6).

3. Seismic reflection data

The subseafloor setting of the Strait of Messina was explored by a tightly-spaced grid (34 profiles, see Fig. 3A) of high-resolution multichannel airgun-seismic lines recorded in December 2011–January 2012 (R/V Meteor, Cruise M86/2). Profiles are variously oriented but mostly of them are transversal to the Strait axis (see supplementary material).

3.1 Seismic-stratigraphy

Although high-resolution seismic data provide excellent constraints on the tectono-sedimentary evolution of the Strait of Messina, only a basic seismo-stratigraphy interpretation is given here according to the aim and topic of the study. The interpretation of the basin-fill seismo-stratigraphic units was therefore performed on selected representative profiles and was based primarily on i) their seismic features (e.g. amplitude, lateral continuity, and frequency of internal reflectors), ii) bounding discontinuities and iii) the depositional architecture. The lithostratigraphic interpretation was supported by available borehole data drilled in the offshore between Messina and Villa S. Giovanni (see Monaco et al., 1996 and Fig. 3B for location), whereas ages were assigned based on correlations with the well-known sedimentary units outcropping on-land on both sides of the Straits (Fig. 3A, see Lentini et al., 2000 and reference therein). Accordingly, seismic units have been labelled from the bottom to the top following the formational names attributed on-land (see Servizio Geologico d'Italia, 2007). In general, the basin-fill sedimentary package is characterized by slope and channel-fill units limited by well-defined discontinuities that have been interpreted as angular and/or erosional unconformities. Seismic facies analysis shows the occurrence of several seismic bodies, spatially variable in thickness, within the up to 0.5 s TWT thick sounded seismo-stratigraphic section (Fig. 4A). The deeper recognized seismic units show low-medium amplitude, laterally discontinuous

310 reflectors, and locally chaotic seismic facies. Its stratigraphic position and drill-hole data in the
311 northern sector of the Straits (Bh4-borehole in Monaco et al., 1996, see Fig. 3C) allow interpreting
312 the seismic body as Tortonian sands and conglomerates, which are also widely outcropping on-land
313 and locally known as the S. Pier Niceto Formation (SPN in Fig. 4B). Upward facing, this unit is
314 locally covered by a seismic body showing chaotic seismic facies, occasionally characterized by
315 isolated and high-amplitude reflectors, and bounded at the top by an undulating discontinuity. The
316 seismic features and the stratigraphic position of the unit enabled us to interpret it as Messinian
317 evaporitic limestones (ELM in Fig. 4B). The Pliocene sediment section lies unconformably above the
318 ELM unit and is characterized by two, variable in thickness, seismic bodies. The lower seismic body
319 occurs discontinuously atop the ELM and consists of a tiny body with semi-transparent seismic facies.
320 According to its stratigraphic position, it has been interpreted as the Zanclean Trubi Formation (TRB
321 in Fig. 4B). The overlying unit is a well-layered seismic body characterized by high-frequency and
322 laterally continuous reflectors with a sub-parallel geometry. This unit shows the greatest thickness
323 (~0.3 TWT) in the western part of the Straits and then gradually decreases towards the east where it
324 generally pinches-out against the lower units. The seismic facies and its position in the sediment
325 column enabled us to correlate the seismic body to the middle-upper Pliocene succession, which is
326 outcropping on-land. This succession encompasses the well-layered alternance of calcarenites and
327 marls of the Rometta formation and the marls of the Massa S. Lucia Formation (RMT+MSL in Fig.
328 4B). A low-amplitude seismic facies occasionally encompassing high-amplitude reflectors
329 characterizes the overlying, ~ 0.1 TWT thick seismic body that, following on-land log sections, has
330 been attributed to the Middle Pleistocene Spadafora Clays (SPC in Fig. 4B). The younger unit is
331 characterized by seismic facies of high-frequency and strongly reflective reflectors generally
332 occurring on the eastern side of the Straits. Its seismic features allow interpreting this seismic body
333 as middle Pleistocene calcarenites of S. Corrado formation (SCC in Fig. 4B). The uppermost seismic
334 unit is characterized by high-frequency, low-to-medium amplitude reflectors with a sub-parallel or
335 occasionally cross-stratified pattern. The seismic facies and stratigraphic level enabled us to interpret

this unit as the Upper Pleistocene Messina gravels and sands Formation (MGS in Fig. 4B). In the eastern part of the Straits, a lens-shaped seismic unit (MGS1) has been interpreted as the basal conglomeratic facies of the Messina gravels and sands Formation.

3.2 Offshore structural pattern

The detailed analysis of seismic-stratigraphy, performed on selected profiles and displaced reflectors observed throughout the entire seismic dataset, enabled depicting the sub-seafloor tectonic setting of the Strait of Messina as well as its through-time evolution. The seismic interpretation was also corroborated by field observation at key sites, which provide an analogue to understand deformation in the offshore. Overall, seismic data interpretation and temporal constraints (see section 3.1) pointed to the investigated sector as being deformed according to distinct tectonic phases, which have been registered by the sediment section. The pre-rifting deformation is recognizable in most of the seismic profiles where a system of folds and reverse faults had involved the Mio-Pliocene part of the sounded seismo-stratigraphic section. Evidence of shortening has been detected mainly off the Sicilian coast where the lower part of the sounded stratigraphic succession is folded and locally displaced by the propagation of several faults with reverse kinematic. Along the P204 line, located between the cities of Messina and Reggio Calabria, shortening has given rise to the development of a short-wavelength (1.5-2 km) system of ramp-anticlines and associated thrusts (Fig. 5A). Thrust propagation folds controlled the deposition of the Mio-Pliocene sedimentary section as demonstrated by the diverging pattern of reflectors on the hanging-wall blocks and sediments thickening at thrust-top-basin depocenters (Fig. 5A). A slightly diverging pattern of reflectors observed also within the ELM (Messinian) and SPN (Upper Tortonian) units, enabled to date the onset of contractional tectonics in the area back to the upper Miocene. Shortening continued during the Pliocene accompanied by the development of a small thrust-top-basin where the Pliocene sediments of the Trubi, Rometta, and Massa S. Lucia Formations (TRB, RMT+MSL, see section 3.1) deposited syn-tectonically (Fig. 5A). Syn-folding deposition of the Pliocene units is also observed along the P217 seismic lines where the

363 folds growth was registered by the diverging pattern of the reflectors within thrust-top synclines (Fig.
364 5B). As revealed by the angular unconformity separating the Pliocene sediments from the overlying
365 units (Fig. 5 B), tectonic shortening in the area vanished at the end of the Pliocene time. Afterward,
366 the no-longer active folded structures were eroded and unconformably sealed by the younger
367 (Pleistocene) seismic units (SPC, SCC, and MGS see section 3.1 and Fig. 4B), as revealed by the sub-
368 parallel pattern of their internal reflectors. Seismic data interpretation and spatial correlation
369 highlighted the contractional feature as having a NE-SW direction, whereas observed folds
370 asymmetry suggests a tectonic transport towards the SE. Detailed age constraints and sediment
371 pattern analysis indicated the investigated sector as having experienced compression up to the
372 Pliocene-Pleistocene transition, therefore confirming previous studies in the area (see Monaco et al.,
373 1996). The occurrence of younger extensional faults overprinting the previous (Miocene-Pliocene)
374 compressional setting accounts for a Quaternary tectonic inversion in the area from which the modern
375 Strait of Messina developed. Extensional tectonic features are widespread all over the investigated
376 sector where the fault pattern depicts an overall asymmetric graben structure extending roughly along
377 the axial zone of the Straits. A major bounding fault (hereinafter the W-fault), has been recognised
378 on the western side of the Strait. It consists of an E-dipping and low-angle (45°) normal fault slicing
379 throughout the sounded sub-seafloor and displacing the seismo-stratigraphic units with variable
380 offsets (Fig. 5C). Minor associated extensional structures occur mainly east of the main W-fault and
381 they consist of small, synthetic and/or antithetic faults generally confined within the Pliocene
382 succession and/or occasionally displacing the base of the youngest units (MGS1, Fig. 5C). Close to
383 the main W-Fault, associated synthetic structures are often characterized by wipe-out zones
384 suggesting fluids ascent through the fault zone. Spatial correlations along the entire seismic dataset
385 allow following the W-fault for a total length of ~20 km in the offshore. It occurs 3.5 km off the
386 Sicilian coast and extends in the offshore from the P230 line (in the south) to the P1007 line (in the
387 north) close to the Calabrian coast (see suppl. Figs. 1, 2, and 3 to follow the fault trace). According
388 to the interpreted seismic-stratigraphy (see section 3.1) and applying time-to-depth conversion, the

389 W-fault has displaced the basal boundary of the Messina Gravels and Sand Formation (MGS1,
390 Middle-Upper Pleistocene, see zooms at the bottom of Fig. 5) of about 80 m as well as the seafloor
391 of the same amount. It is worth noting that the W-Fault emerges at the seafloor right where previous
392 authors (Ridente et al., 2014) observed/mapped triangular facets and suspended incisions along the
393 most rectilinear portion of the Messina canyon. Quaternary faulting in the eastern side of the Straits
394 has only been inferred from the occurrence of some scarps at the seafloor. Although scarps roughly
395 correlate with the offshore continuation of some tectonic structures mapped on-land (i.e. the Armo
396 and Reggio Calabria faults, see Fig. 1D), clearly displaced reflectors were not observed at depth in
397 the sub-seafloor setting. Seafloor scarps have been observed only along the P231 and P233 seismic
398 lines, located in the southern portion of the Straits (Fig. 3A), whereas neither evidence for faulting
399 nor seafloor scarps have been recognized to the north approaching the Calabrian coast at the ideal
400 offshore continuation of the Reggio Calabria Fault (suppl. Fig. 2 b-c). Noteworthy, the easternmost
401 portion of the P230, P231, and P233 seismic lines in the Calabrian side roughly illuminate the same
402 sector explored by previous authors where an active fault displacing the seafloor was considered to
403 be the seismogenic source for the 1908 earthquake (i.e. the South Calabria Fault, see Line Tao17 in
404 Argnani et al., 2009). However, by applying time-to-depth conversion and removing vertical
405 exaggeration from the high-resolution seismic lines covering the same area, the dip-angle of both the
406 seafloor fault-scarp and of the accounted sub-seafloor fault trace reduce notably to 15-20°.
407 Accordingly, the seafloor scarp could represent the frontal portion of a submarine landslide (see also
408 Ridente et al., 2014) and the inferred sub-seafloor fault trace a Messinian in age paleo-slope above
409 which the Pliocene sediments deposited unconformably (suppl. Fig. 3 b-c).
410 Seismic interpretation over the analysed seismic dataset confirms that the shallow portion of the Strait
411 of Messina area was controlled during the Quaternary by the propagation of extensional faults. In this
412 frame, the previously unmapped W-Fault displaced the seafloor and appears as/proves to be the most
413 evident tectonic structure in the area. Conversely, seismic imaging in the Calabrian side rules out a

414 continuation in the offshore of the Armo and Reggio Calabria faults and appear to disprove the
415 occurrence of the South Calabria Fault (see Argnani et al., 2009).
416
417 *3.3 The continuation on-land of the W-fault*
418 Seismic data interpretation pointed to how the W-Fault represents the first evidence of Holocene
419 deformation in the area. However, while its southern tip can be placed certainly between the line P230
420 and P231 (see Fig. 3A), its northward continuation is poorly constrained since the fault plane bends
421 to the east pointing straight toward the Calabrian mainland where fault orientation roughly fits with
422 the Catona River mainstream (Fig. 6A). To support its continuation on land across southern Calabria,
423 morpho-structural features were investigated along the drainage basin of the Catona River, a large
424 ENE-WSW trending fluvial system flowing towards the Strait of Messina. Landscape analysis was
425 supported by a high-resolution (5x5m cell size) DTM (http://geoportale.regione.calabria.it/opendata)
426 and by 1:10.000-scale aerial photographs. Climate cycles coupled with regional and local uplift gave
427 rise to the development of a flight of Pleistocene alluvial-marine terraces in the area (Miyauchi et al.,
428 1994; Monaco et al., 2017 and references therein), which are currently well-preserved out-of-water
429 along the flanks of the Catona drainage basin at variable altitude (Fig. 6A). Altitude distribution of
430 the accurately re-mapped basal boundary of the terraces and age constraints (Bonfiglio, 1972;
431 Bonfiglio and Violanti, 1983; Dumas et al., 1987; Balescu et al., 1997) were then taken as reference
432 points to detect possible deformation in the area. Geological profiling over the high-resolution DTM
433 revealed that all the terraces preserved in the southern flank of the Catona drainage basin are
434 systematically tilted toward the North whereas, in the northern flank, they lie at a higher topographic
435 altitude. Previously mapped faults in the area bordering the northern flank of the Catona drainage
436 basin (i.e. the Campo Piale high, see Monaco et al., 2017 and reference therein), could have
437 contributed in the past both to enhance terraces uplift on its footwall and compensate it in the hanging-
438 wall where 167 and 200 ka-old terraces are preserved. In general, altitude distribution and tilting of
439 the terraces in the area result in a miscorrelation between climate markers of the same age located at

the northern and southern flanks of the Catona drainage basin, respectively (Fig. 7). This arrangement strongly suggests the occurrence of a tectonic structure in-between. Tectonic control along the river is also suggested by the absence in the south of the 100 and 330-ka terraces suggesting a differential uplift between the two flanks of the drainage system. Further, an evident fluvial deflection has been observed on the northern flank of the Catona fluvial valley NW of S. Roberto village. Here, a tributary WNW-ESE trending fluvial incision, locally known as V.ne Passo dei Limbi, has been strongly deflected by about 90°, hence changing its direction from N115E to N45E (V.ne Funica, see inset in Fig. 6B). The displaced 410-ka marine terrace (see profile n. 8 in Fig. 7) clearly suggests that fluvial deflection has been controlled by a NE-SW trending fault segment occurring right along the V.ne Funica. The undisturbed, 900-ka old terrace in the eastern sector of the Catona fluvial valley (see profile n. 9 in Fig. 7), excludes faulting continuation in this area, supporting fault plane bending to the NE along the Funica fluvial incision. Tilted-to-dislocated marine terraces and observed fluvial deflections along the Catona fluvial valley therefore supports a continuation of the W-Fault on-land in southern Calabria. Finally, by joining the offshore and the on-land segment, an orientation consistent with the coastline trend of the Strait of Messina is achieved for the W-Fault.

4. Seismological data

4.1 Earthquakes

The analysis of national and local earthquake catalogues has pointed that about 2700 low-magnitude ($0.6<M<4.3$) earthquakes originated in the studied region in the last 40 years (1981-2018). The re-located seismic events are distributed mainly between the Ionian coast of NE Sicily and the Calabrian mainland whereas a substantial lack of crustal seismicity is observed to the west, beneath Sicily and south of the Straits, in the Ionian offshore (Fig. 8A). About 20 km further south, seismic activity resumes along the NW-SE Aeolian Islands-Ionian Sea Fault System (Scarfì et al., 2016, 2018; Barreca et al., 2019). Events clustering is observed along the Sicilian coastal domain close to the city of Messina and about10 km further south in the offshore where a NNE-SSW trending cluster of events

467 (see also Scarfì et al., 2009) aligns well with the trace of the active W-Fault (Fig. 8A), as mapped by
468 seismic interpretation in the axial zone of the Straits (see section 3.2). To the east, in mainland
469 Calabria, earthquakes appear to roughly follow the main NE-SW trending Quaternary morpho-
470 structural features occurring in the area. Earthquakes gather mainly at the overlapping sector between
471 the Armo and Cittanova faults (Fig. 8A). The 3D-view of earthquakes reveals how seismicity is
472 distributed at depth in the crustal domain. Of note, depth-distribution of events pointed to a wedge-
473 shaped seismogenic volume beneath the investigated sector, which is limited downward by an evident
474 cut-off of seismicity (Fig. 8B). Most likely, the discontinuity in the seismicity pattern accounts for a
475 brittle-ductile transition (BDT) that separates a rigid (seismogenic) overlying block from a much less
476 rigid (almost non-seismogenic) underlying block. The transition delineates roughly a low-angle and
477 SE-dipping possible crustal discontinuity occurring at depth between the Strait of Messina (6 km-
478 depth) and southern Calabria (18 km-depth). In this frame, the previously described clusters (i.e.
479 below the Strait of Messina seaway) localize above the seismicity cut-off where they appear to
480 delineate steeper tectonic structures (Fig. 8B). Events distribution beneath southern Calabria seems
481 to follow the projection at depth of the Armo fault, whereas no seismicity is associated with the
482 Reggio Calabria fault. Information on the current kinematics affecting the investigated sector have
483 been achieved by the analysis of available focal solutions (see Scarfi et al., 2020 and Supplementary
484 Table IV). Seismic faulting in the area is mainly characterized by normal kinematics in the depth-
485 range 5-15 km, whereas rare and deeper earthquakes (10-50 km) show strike-slip and oblique-reverse
486 kinematics (Fig. 8A). Along the central portion of the Strait of Messina and in southern Calabria,
487 nodal planes are mainly oriented NNE-SSW even if they change direction to E-W at the north-eastern
488 corner of the Strait of Messina along the Catona drainage basin (see section 3.3). Although beneath
489 the Strait of Messina the events clustering suggests the occurrence of very steep tectonic features, the
490 nodal planes of associated focal solutions (including the 1908 event) show dip-angle in the range 45-
491 55°, compatible with the inclination of the W-Fault (see section 3.2). The resulting seismotectonic
492 picture is that of seismic faulting mainly occurring within the wedge-shaped seismogenic volume

493 along moderate-dipping fault planes connecting downward on the deeper foreland-dipping
494 discontinuity (Fig. 8C). A stress tensor model for the investigated sector was achieved by the
495 inversion of the selected fault planes solution. By using the STRESSINVERSE software (Vavryčuk,
496 2014), and according to the method proposed by Michael (1984, 1987) and Lund and Slunga, (1999),
497 a sub-vertical (88°) principal stress tensor (S1) and horizontal (2°), NW-SE striking minimum S3
498 were resolved (Fig. 8D), confirming extensional regime in the area.

499 *4.2 V_p tomographic model*
500
501 Vertical sections through the available V_p model (see Scarfì et al., 2018 and suppl. Fig. 4 for the
502 uninterpreted V_p sections) have been selected to explore the lithospheric structural architecture of the
503 investigated area. The geophysical data consist of four NW-SE oriented lithospheric sections passing
504 orthogonally to the forearc-trench region of the Ionian Subduction Zone down to a depth of 60 km
505 (Fig.9A). The Moho discontinuity is identified where P-wave velocity of 7.6–7.8 km/s is exceeded
506 (see Rabbel et al., 2013). Tectonic interpretation allows imaging the geometry of the shallow portion
507 of the subduction system where the Ionian oceanic lithosphere is underplating the Calabrian
508 continental backstop (Fig. 9B and C). Following the Tyrrhenian Moho geometry in the upper plate of
509 the system it is possible to note that, above the subduction hinge, the European plate is strongly folded
510 upwards to form an asymmetric lithospheric culmination right below the Peloritani Mts (NE Sicily).
511 In this frame, it is likely that extensional deformation in the investigated sector has been favoured by
512 the lithospheric warping, sustaining uplift and extrados stretching in NE Sicily and tectonic collapse
513 to the east along the Strait of Messina and southern Calabria. The discontinuity inferred by the cut-
514 off in the crustal seismicity (see section 4.1) falls along the E-facing and steepest limb of the
515 lithospheric culmination roughly fitting with its inclination. The occurrence of a low-angle and E-
516 dipping discontinuity within the reconstructed tectonic setting shows similarities with the structural
517 architecture of the Umbria–Marche sector of the Northern Apennine thrust belt (Fig. 9D) where the
518 active, low-angle Alto Tiberina Fault occurs (see Barchi et al., 1998; Boncio et al., 2000).

5. Data analysis from 3D modelling

Stratigraphic and tectonic interpretation from high-resolution seismic lines, along with relocated earthquakes and seismic tomography, provides an opportunity to better understand the tectonic pattern of the investigated area down to sub-crustal depth. To have a comprehensive view of all analysed data and particularly on the spatial correlations between tectonic and seismological features, a simplified but consistent three-dimensional model was built up by using Move 2019.1 geo-modelling software package (Petex Ltd). Structural interpretation and spatial interpolation of faults picked along the entire 2D seismic dataset (see section 3.2), and on-land morpho-structural data enabled us to depict the shallow structural pattern characterizing the Strait of Messina (Fig. 10A). Sub-surface 3D geometry of the shallow faults was achieved by extruding them along-dip up to the seismogenic depth and maintaining fixed their dip-angle. Modelling revealed the W-Fault (onshore+offshore) as an N50E trending tectonic feature dipping towards the ESE (N135E) at 45° and characterized by a bend toward the west of the non-linear fault plane. Since seismic imaging does not support offshore continuation for the faults occurring in the Calabrian side of the Straits (i.e. the Armo and Reggio Calabria Faults), we only modelled their onshore expression considering as geometric constraints the field data provided by previous authors (Ghisetti, 1992; Tortorici et al., 1995). Modelling suggests both the Reggio Calabria and Armo faults as a N20E striking and W-dipping (N300E) tectonic structures having a length of 14 and 25 km, respectively (Fig. 10A). Modelling for these two faults was necessary to test again their reliability as a potential source for large earthquakes in the area (see section 5.1). Hypocentres distribution of relocated earthquakes in the area (see section 4.1) may suggest the existence of a rheological boundary at depth within the crustal domain. Serial (2.5 km spaced) profiles performed across the Straits and earthquakes projection (within ± 2.5 km from the profiles traces, see suppl. Fig. 5) allow modelling the possible 3D plane roughly fitting the cut-off of seismicity. Finally, modelling resolved a 30x24 km-wide discontinuity dipping towards the SE at an angle of about 24° (Fig. 10B). To frame the modelled

545 shallowest tectonic features in the larger context of the Africa-Europe plate convergence, a schematic
546 3D-model of the deeper subduction system was also provided by interpolating the Tyrrhenian Moho
547 discontinuity and the top-slab surface of the descending African plate as traced on the available
548 seismic tomography (see Fig. 10C). As stated above (see section 4.2), seismic tomography evidenced
549 a significant up-bending of the upper plate block. 3D-interpolation highlight a dome-shaped uplift of
550 the upper plate localizing above the slab-hinge zone and right beneath the Sicily mainland (Fig. 10
551 C). Modelled top-slab surface and Tyrrhenian Moho discontinuity highlights how the lithospheric
552 uplift is more marked right where the slab is more inclined (Fig. 10C) suggesting, therefore, a link
553 between differential slab retreat dynamics and fore-arc mantle upraise (see also Doglioni et al., 1999,
554 2009). 3D modelling of all features therefore provides an opportunity to explore the geometric and
555 kinematic relationships between deep-seated geodynamic processes and deformation in the upper
556 portion of the crust (Fig. 11). According to the regional setting of the Calabrian Arc, the foreland-
557 dipping low-angle discontinuity highlighted by the rheological transition (seismogenic vs non-
558 seismogenic, see Fig. 8B and C) can be interpreted as an old decollement level originally separating
559 a rigid hanging-wall block (crystalline) from under-thrusted and less rigid sediments. Subsequently,
560 the old decollement was folded and tilted following the upper plate asymmetric doming just to the
561 west until to be placed in the current foreland-dipping position at the steepest eastern limb of the
562 lithospheric culmination (Fig. 11B).

563 Vignaroli

564

565 In this setting, possible reactivation of the old decollement as a low-angle detachment fault could
566 therefore be favoured by sliding eastward of its hanging-wall block under the gravity and tectonic
567 forces. (see section 6). The reconstructed geometric relationships and a kinematic linking between
568 the low-angle plane and faults pattern in the overlying Strait of Messina were predicted by analogue
569 modelling performed for the area. According to the sand-box experiment (see Bonini et al., 2011),

570 simulated slip on the low-angle structure supports tectonic collapse and graben formation in the zone
571 above its shallowest tip and along the hanging-wall block.

572 ## 6. An alternative model to explain subsidence and seismic rupture in the area

573 Although roughly modelled from the seismicity cut-off, the low-angle discontinuity here evidenced
574 is consistent with the E-dipping source models imaged for the 1908 Messina-Reggio Calabria
575 earthquake by previous authors (e.g. see Amoruso et al., 2002 and reference therein). However,
576 frictional fault reactivation theory predicts that slip on low-angle normal faults (LANF <30°, see
577 Wernicke, 1981) is unlikely since movement on such faults requires contradicting the Anderson
578 theory (Anderson, 1951; Sibson, 1985). Likewise, seismic vs. aseismic mechanical behaviour of
579 LANFs has long been debated since large earthquakes along such kinds of structures are rare in the
580 seismological record. Conversely, worldwide examples also suggest that LANFs could occasionally
581 have a brittle-frictional nature and thereby capable of generating M > 6 earthquakes (see Axen, 1999
582 for an overview). Although our modelled low-angle plane could be dimensionally capable (30x24
583 km-wide) of generating M~7 earthquakes, the observed cut-off in the seismicity suggests how it could
584 mark a brittle-ductile transition (BDT) since it appears to separate a rigid (seismogenic) overlying
585 block from a much less rigid (almost non-seismogenic) underlying block (Fig. 9). By using the stress
586 analysis tools of Move 2019.1 software (Petex, Ltd), the stress tensors derived from the inversion of
587 earthquake focal solutions (see section 4.1 and Fig. 8D) were remotely applied to the modelled low-
588 angle surfaces. Considering an average density of 2700 kg/m^3 for the crystalline rocks and
589 approximating the vertical max stress (S1) to the lithostatic load, an overburden pressure of about 320
590 MPa is resolved at a mean depth (12.5 km) in the medium around the low-angle modelled plane (Fig.
591 12A). According to the dip-angle of the discontinuity (24°) and to the applied lithostatic load, slip
592 tendency analysis (τ/σ_n ratio, see Fig. 12 B) revealed that the low-angle discontinuity is an almost
593 mechanically stable plane in the confining effective normal stress field (i.e. the normal stress minus
594 fluid pore pressure), considering a typical angle of internal friction (φ) of 30° (see inset 1 in Fig.

595 12A). Nonetheless, a comparison between the N-S extension of the low-angle discontinuity with the
596 first-order wavelength of the observed subsidence (Fig. 12 C) suggests a cause-and-effect relationship
597 between a possible movement on the discontinuity and measured surface deformation. The ideal
598 projection at the surface of the modelled discontinuity in fact revealed a good fit between its north-
599 eastern and south-western limits and ground elevation changes from positive to negative (Fig. 12C).
600 In this view, a possible movement on the low-angle plane can be assumed only for values of the
601 internal friction (φ) lower than 26° (see inset 2 in Fig. 1A) or, alternatively, for values of the
602 coefficient of internal friction (μs) lower than 0.48. Since a μs < 0.48 is out of the typical μs range for
603 most brittle rocks (0.6-0.8, see Byerlee, 1978; Jaeger and Cook, 1979), possible movement on the
604 low-angle structure is expected only according to a mechanical weakness of the discontinuity where
605 aseismic creeping or stable sliding is more likely than stick-slip behaviour (see Collettini et al., 2009;
606 2011). Several studies have suggested that some mature crustal faults are weak compared to
607 laboratory friction values (Zoback, et al., 1978; Rice, 1992; Byerlee, 1978). This assertion is in line
608 with the tectonic history inferred for the low-angle fault, a former decollement tilted by the upper
609 plate doming (see section 6 and Fig. 11B). Further, no uplift recorded by the levelling data (see
610 Loperfido, 1909) at the ideal footwall-block of the low-angle discontinuity (i.e. in the Peloritani Mts.
611 Fig. 2B) appears in contrast with a tectonically-driven fault movement. At Capo Peloro, in the
612 northern end of the Straits (see Fig. 13A for location), the projection at the surface of the NE corner
613 of the modelled low-angle plane matches well with the negative ground elevation changes detected
614 in the area by the high-precision levelling network (Spampinato et al., 2013). Data levelling revealed
615 a constant deformation trend during the last 40 years, suggesting the NE-corner of Sicily as a low-
616 rate subsiding area above the modelled low-angle plane. According to Doglioni et al. (2005), low
617 friction rocks may easily slip, and in active tectonic settings, they tend to be associated with higher
618 strain rates. High strain rate in the order of 120 nano-strain/yr has in fact been resolved along the
619 Strait of Messina area (Mattia et al., 2009; Serpelloni et al., 2010) where the interseismic strain has
620 been modelled to be produced by a 3.5 mm/yr motion along a low-angle and E-dipping discontinuity

621 (Serpelloni et al., 2010). All these issues, together with the weak assumption that measured ground
622 variations are doubtless coseismic, therefore open new perspectives on the deformation process that
623 caused surface deformation and lead us to propose a previously unexplored model to explain ground
624 elevation changes, stress perturbation, and earthquake triggering in the area. The model exploits the
625 3D reconstructed geometric relations between the deep-seated low-angle discontinuity and the
626 overlying faults (i.e. the W-Fault, Reggio Calabria, and Armo faults, see section 6 and Fig. 11A) and
627 foresees the possibility that an almost aseismic slip event, possibly gravity-driven (see Doglioni et
628 al., 2005) and probably occurring along the low-angle discontinuity just before the 1908 mainshock,
629 may have mechanically destabilized the overlying and already tectonically stressed brittle faults
630 therefore inducing them to rupturing in large earthquakes along the Strait of Messina region according
631 to their dimensions.
632
633 *6.1 Testing the model*
634
635 To kinematically validate the proposed deformation model, the 3D modelled geometries and nearby
636 relationships between the low-angle discontinuity and the overlying faults (i.e. W-Fault, Reggio
637 Calabria, and Armo Faults) were used as input data to simulate i) low-angle fault-induced vertical
638 displacements on the Strait of Messina topography and ii) the response of shallow faults to the same
639 stress perturbations following the Coulomb stress-transfer criterion. Results have been then exploited
640 to perform elastic dislocation models (Okada, 1985) aimed at comparing the expected surface
641 displacement from both the source fault (i.e. the low-angle discontinuity) and the mechanically
642 solicited receiver shallow faults with the ground subsidence observed after the 1908 mainshock.
643
644 *6.1.1 Coulomb Stress Changes modelling*
645 According to the Coulomb stress-transfer criterion, along-fault discrete deformation and associated
646 earthquakes may result in a local stress re-distribution in the fault-surrounding rock volume and in a
647 perturbation of the shear and normal stress acting on nearby tectonic structures (King et al., 1994). In

addition to being governed by the mechanical properties of the medium, failure and earthquake nucleation on nearby faults can also be encouraged where Coulomb Stress Change (hereinafter CSC) is positive (> 0.1 bar) or vice versa discouraged if induced stress change is negative (see Stein, 1999 and Anderson and Johnson, 1999 for an overview). The Coulomb stress change is defined as $\Delta CFF = \Delta\tau + \mu'\Delta\sigma_n$, where $\Delta\tau$ is the change in shear stress (positive in the slip direction), $\Delta\sigma_n$ is the change in normal stress (positive when the fault is unlocked), and μ' is the apparent friction coefficient after accounting for the pore fluid pressure effect (see Reasenberg and Simpson, 1992). Assuming as plausible the existence of a cause-and-effect relationship between the movement on the low-angle discontinuity and the measured ground elevation changes (see section 6), we simulated a normal dip-slip displacement on the 3D foreland-dipping fault and then compared the predicted displacement field on the Strait of Messina topography with the elevation changes measured after the 1908 mainshock (Loperfido, 1909, Figs. 2B and 13 A). Considering previous accounts on the mechanical behaviour of the low-angle discontinuity, a zero cohesive strength and an average μs of 0.4 is assumed at the low-angle fault to simulate a real-world scenario. A Young's Modulus of 75 Gpa is obtained by the following equation:

$$Vp = \sqrt{\frac{E}{\rho}}$$

where V_p is the average P-wave velocity (5.3 Km/s) as obtained by the available V_p model, E is the Young's Modulus and ρ is the bulk density (2700 Kg/m^3). Using a trial-and-error approach and realistic fault surfaces, topography response modelling was obtained by directly incrementing slip magnitude until the predicted displacement matched with the first-order wavelength of the observed subsidence. The best-fits are achieved for a magnitude of the applied normal slip between 1 and 1.8 [m] that produced a maximum topographic variation of -0.7 m at the centre of the Strait of Messina and along its coastal sectors (Fig. 13A). Uplift in the order of 0.15 [m] is also predicted to occur in much of southern Calabria above the basin-ward tip (-18 km) of the low-angle discontinuity whereas

672 a slight subsidence is expected along the Peloritani Mts. in Sicily. Along the southern coast of
673 Calabria, predicted uplift and subsidence match well with the positive to negative ground changes
674 evidenced by the levelling data. The maximum slip magnitude (1.8 m), achieved from the above
675 forward simulation was again used to generate stress perturbation in the elastic medium surrounding
676 the low-angle discontinuity and to evaluate the response of the overlying brittle faults (i.e. the W-
677 Fault and Armo fault). Using the detailed 3D fault configuration (Fig. 13B), CSC transfer between
678 the deep-seated and shallow structures was therefore investigated by setting the low-angle
679 discontinuity as a source fault and the overlying W-Fault and Armo as receiver faults. The Reggio
680 Calabria Fault was excluded from the computation since, given its length, a large earthquake such as
681 the 1908 event cannot be generated by this structure. A regional stress field, achieved from the
682 inversion of focal solutions (see section 4.1 and Fig. 8D), was also applied to the shallow fault system
683 to evaluate the background stress state on the fault planes. Shallow faults were assumed as
684 cohesionless and a typical coefficient of internal friction (μ_s) of 0.4 was considered at the fault core
685 (King et al., 1994). Forward modelling predicts an additional positive Coulomb induced stress (max
686 3.2 bar) along much of the W-Fault (Fig. 13C), whereas negligible stress is transferred to the Armo
687 Fault (Fig. 13 D). Considering the available focal solution for the 1908 earthquake (see Fig. 8A), the
688 induced CSC related to pure slip-motions (normal, left-lateral and right-lateral dislocation; Aki and
689 Richards, 1980), was also investigated for the more destabilized W-Fault. The analysis of the CSC
690 transfers on faults for the specified rake revealed the shallow portion of the W-Fault as potentially
691 capable of slipping for much of its length following a normal oblique left-lateral motion (Fig. 13 E
692 and F), while a right-lateral motion is possible only on a small area at its northern tip (Fig. 13G).
693 Although stress perturbation caused by the slip on the low-angle discontinuity is not able to
694 destabilize the Armo fault, we tested the possibility of failure along such structure by forwarding a
695 large earthquake on the nearby and potentially unstable W-Fault. Considering the length (34.5 km)
696 of the W-Fault, CSC transfer analysis was operated by simulating 2.5 m of normal dip-slip motion
697 on the structure, the maximum expected displacement derived from empirical-scale relationships (see

698 Weels and Coppersmith, 1999, Leonard, 2010) according to a seismic event of M ~ 6.9. Computed
699 CSC also revealed in this case that negligible positive stress is transferred to the Armo Fault for fixed
700 pure slip-motion (Fig. 13 H-L). Overall, the CSC analysis therefore supports the proposed alternative
701 model in which an almost aseismic slip on the low-angle discontinuity can mechanically destabilize
702 the overlying faults. However, results suggest that stress perturbation induced by the slip on the low-
703 angle discontinuity is mainly transferred to the W-Fault where Coulomb pressure exceeding 3 [bar]
704 provides conditions for fault failure and earthquake triggering.

705

706 *6.1.2 Inversion of levelling data by multiple sources*

707 As evidenced by Aloisi et al. (2013), modelling on available levelling data (Loperfido, 1909) does
708 not constrain a unique model solution for the 1908 earthquake, since they are not suitable for
709 differentiating between W-dipping faults on the Calabrian side from E-dipping faults on the Sicilian
710 side of the Straits. To further validate our proposed deformation model (see section6), we sought to
711 answer the question if the levelling data could be the result of multiple dislocations along different
712 sources and not the exclusive consequence of a coseismic slip along a single fault. Remarking the
713 results from the CSC analysis, which showed that normal and left-lateral dislocations are encouraged
714 along much of the W-fault, an analytical inversion of the levelling data using a rectangular dislocation
715 model (Okada, 1985) and multiple sources has been performed. Analytical inversion was run through
716 the Pattern Search technique together with local Genetic Algorithm Search and nonlinear least-
717 squares optimization (Cannavò, 2019). A jackknife resampling method (Cannavò, 2019) was also
718 adopted to estimate the uncertainty of each parameter. Effects of the topography were not considered
719 in the data inversion since they have no influence on data output because of the large extension of the
720 investigated area compared to the mountain range elevations and to the kind of recorded data. The
721 medium was assumed to have a typical Poisson ratio of 0.25. Dislocation modelling was performed
722 in an elastic, isotropic, and homogeneous half-space by considering for each structural discontinuity
723 the spatial coordinates, dimensions, dip-angle, and finally the dislocation components (normal and

724 left-lateral are positive in Tab. 1). To obtain a more realistic configuration of the faults, the non-linear
725 W-fault plane was split into four patches (Fig.14 A). In the computation, levelling benchmarks on the
726 Sicilian side were excluded because the chosen referring point (S. Rizzo hill, see Fig. 13A for
727 location) is probably too close to the area affected by the subsidence (Loperfido, 1909). Keeping
728 locked all the fault parameters except for the dip-slip dislocation component (Tab. 1), data inversion
729 was firstly performed by applying a dip-slip motion to the low-angle discontinuity to simulate sliding
730 toward the east. Results suggest that a dip-slip normal dislocation of about 1.1 [m] is enough to
731 reproduce the first-order wavelength of the observed subsidence pattern (Fig. 14B). It is noteworthy
732 that the previously described trial-and-error approach (see section 6.1.1) provided that a motion in
733 the range of 1-1.8 [m] on a more realistic representation of the low-angle discontinuity and using a
734 real topography can explain the subsidence provided by the levelling data. Inverting the levelling data
735 using a simplified representation of the faults, we obtained a value (1.1m) within that range.
736 Following the results coming from the CSC analysis, we verified if the observed levelling data pattern
737 is better reproduced in the "second-order" variations by adding the effects of dislocations along the
738 faults located above the low-angle discontinuity (i.e. the W-fault, Reggio Calabria, and Armo fault).
739 Considering the geometrical parameters of the overlying faults (Tab. 1) and the slightly oblique
740 extensional stress field (see Fig. 8D), levelling data inversion was performed by accounting only for
741 the lateral and dip-slip components of motion. The parameter search range for the normal component
742 was limited to the maximum displacement (4.89 m) expected from a 7.1 magnitude earthquake as
743 estimated for the 1908 seismic event. According to the focal solution available for the 1908 event and
744 considering the E-dipping nodal plane (see Fig. 8A), the left-lateral component was limited to 35%
745 of the maximum normal component. An excellent fit between calculated and observed ground
746 variations is then resolved through the activation of the low-angle discontinuity and the overlying
747 faults (Fig. 14B). The computed modules of the dislocation's components for the shallow faults (Tab.
748 1), revealed that deformation on the W-fault is dominant with a normal component of about 4.5 [m]
749 and a left-lateral component of 2.3 [m] on its southernmost portion. As indicated also by the CSC

750 analysis, the inversion of levelling data again suggests the negligible role of the Armo fault in
751 producing ground variations since a normal dip-slip dislocation of 0.028 m is achieved (Tab. 1).

752 ## 7. Discussion

753

754 ### *7.1 The reliability of the W-Fault as a causative fault for the 1908 seismic event*

755 Seismo-stratigraphic and tectonic interpretation over the dense grid of seismic lines revealed how the
756 shallow portion of the Strait of Messina has been shaped by an array of Quaternary extensional faults
757 overprinting a previous Mio-Pliocene compressional setting. Overall, the activity of the younger
758 faults has deformed the area according to an asymmetric graben structure, giving rise to the modern
759 Strait of Messina. However, marine geophysical investigations revealed that while in the western
760 (Sicilian) side of the Straits Quaternary faulting is quite evident, the offshore continuation of the faults
761 slicing across southern Calabria (i.e. the Armo and Reggio Calabria faults, see Fig.1 D) is not clearly
762 supported. In the western side, about 3 km off the Sicilian coast, an NNE-SSW trending extensional
763 fault (the W-Fault) has been found to propagate through the whole sounded sub-seafloor setting. The
764 tectonic structure has also considerably deformed the seafloor by about 80 m, providing therefore
765 first evidence of Holocene rupture in the area. A morphotectonic analysis was performed in southern
766 Calabria following the orientation of the W-Fault as mapped in the offshore. Tilted-to-dislocated
767 marine terraces and fluvial deflections strongly support a continuation of the W-Fault on-land in
768 southern Calabria right along the Catona River fluvial valley (see section 3.3). By merging the two
769 segments of the W-Fault, a previously unknown 34.5 km-long active tectonic structure is therefore
770 evidenced in the Strait of Messina area (Fig. 15). According to the empirical-scale relationships
771 (Wells and Coppersmith, 1994; Leonard, 2010), the fault has the potential to generate an M~6.9
772 earthquake, which is the minimum estimated magnitude for the 1908 earthquake. Noteworthy, the
773 surface expression of the mapped W-Fault well overlaps with observed severe damage (Baratta, 1910)
774 and with the zone where the higher concentration of ground fracturing was reported (see Blumetti et
775 al., 2008 and Fig. 15). The breaking of a submarine telephone cable crossing the Straits (between

776 Gallico in Calabria and Gazzi in Sicily, see Comerci et al., 2008 and Fig. 15 for location) during the
777 1908 earthquake further suggests that surface rupture may have occurred offshore right along the W-
778 Fault. According to the proposed deformation model (see section 6) and the CSC analysis, stress
779 perturbation by a probable aseismic slip event on the low-angle discontinuity resolved additional
780 Coulomb stress along the W-Fault. The potentially induced transtensional slip for much of the W-
781 Fault length (see Fig. 13 E-G) fits well with the kinematic rupture of the 1908 seismic event as
782 provided by the available focal solution. Geodetic data inversion by multiple sources (see section
783 6.1.2), finally suggested that an excellent fit between the calculated and the observed subsidence is
784 resolved by simulating a 1.1 m of normal displacement along the low-angle discontinuity and a left-
785 lateral transtensional motion of ~ 5 m (4.5 m normal slip and 2.3 m left-lateral slip) along the W-
786 Fault, a displacement value that is compatible with an M~7 earthquake. All these issues strongly
787 suggest the W-Fault as the best candidate to have produced large earthquakes in the Strait of Messina
788 area. As documented by historical reports and observations (Platania, 1909), a huge tsunami
789 inundated the Calabrian and Sicilian coastlines a few minutes after the mainshock event. Modelling
790 of runup and arrival data are is favour of a submarine landslide source in the southern sector of the
791 Strait (Billi et al., 2008, 2010). This imply that the causative fault of the 1908 earthquake can be
792 limited in its extent to the Strait of Messina area, therefore supporting the location here provided for
793 the W-Fault. Moreover, seismic rupture and significant shacking are also expected by coulomb stress
794 change (see also Billi et al., 2008) at the tips of extensional faults and, accordingly, mass failure in
795 the nearby are encouraged where the slope is steep enough. This assertion agrees with the submarine
796 landslide location provided by previous authors (e.g. Billi et al., 2008, 2010), which is close to the
797 southern tip of the W-Fault. In addition, a new composite source has been recently proposed to explain
798 tsunami in the Strait of Messina area (see Schambach et al. 2020). Results from simulation point to a
799 double-source (mass failure + seafloor rupture) substantially confirming the location of previously
800 reported submarine landslide (see Billi et al., 2008; 2010) and a coseismic rupture along the Strait.
801 However, since the occurrence of the seismic source selected for the tsunami modelling (i.e. the 70-

802 km long MTF, see Meschis et al., 2019, and Fig. 1D for location) is disproved by the high-resolution
803 seismic investigation (see section 7.2), it is likely that the seafloor rupture was charged by the
804 constrained W-Fault.

805 *7.2 Questioning the previously inferred 1908 causative faults and models*

806 By taking advances from i) the high-resolution seismic imaging covering much of the Strait of
807 Messina, ii) the distribution of crustal seismicity and V_p model, iii) fault dislocation modelling and
808 stress analysis, a critical review of the previous hypothesis concerning the 1908 causative fault is set
809 out here. In addition to providing evidence for surface faulting along the W-Fault, seismic imaging
810 also concurred to weaken or disprove previous inferred causative faults located in the offshore. The
811 P231, P230 and P233 seismic lines in the southern sector of the Strait of Messina, clearly illuminate
812 the Calabrian side of the Strait. The lines cover the region of the possible continuation of the Armo
813 and Reggio Calabria faults offshore as well as the area where previous authors mapped an active fault
814 (i.e. the South Calabria Fault, see Argnani et al., 2009). Although the occurrence of some high-angle
815 seafloor scarps seems to support active faulting in the area, time-to-depth conversion of the seismic
816 lines and no vertical exaggeration applied, revealed how the slope degree of the scarps is reduced
817 notably to 15- 10°. Accordingly, the seafloor scarps likely represent the frontal portion of submarine
818 landslides (see also Ridente et al., 2014) rather than seafloor dislocation produced by active faults, as
819 also supported by the absence of sub-seafloor displaced reflectors (see suppl. Fig. 3 B and C). In this
820 view, the offshore continuation of the Armo and Reggio Calabria faults is therefore disproved, as is
821 the occurrence of the South Calabria Fault (SCF in Fig. 1C), the latter inferred to be the seismogenic
822 source of the 1908 earthquake (see Argnani et al., 2009). Strong seismotectonic implications stem
823 from the non-continuation in the offshore of the faults slicing across southern Calabria since their
824 seismic potential must be reduced in the light of their minor length. Seismic imaging in the Sicilian
825 side enabled us to also question a recently published paper (Meschis et al., 2019) concerning new
826 source modelling in the Strait of Messina. According to the authors, the 1908 earthquake was caused

827 by a coseismic slip on a 70 km-long mapped fault, the so-called Messina-Taormina Fault (MTF in
828 Fig. 1D and model in Fig. 2D). However, the occurrence of such a long fault off the Sicilian coast,
829 inferred only on the basis of a few raised coastal marine terraces in the Sicily mainland (De Guidi et
830 al., 2003), seems to be disproved by the high-resolution seismic investigation as well as by previous
831 studies in the area (see Argnani, 2009; Barreca et al., 2019). Neither evidence for faulting nor seafloor
832 scarps have in fact been observed along the P231and P233 lines in the southern portion of the Strait
833 and crossing the mapped MTF (suppl. Fig. 3 A, B, and C).
834 Hypocentres of earthquakes have suggested the occurrence of a rheological boundary at depth within
835 the crustal domain. Following similar tectonic patterns evidenced all along the Apennine Chain (e.g.
836 the Altotiberina faults, see Barchi et al., 1998 and Fig. 9D), we infer this discontinuity to be an
837 extensional low-angle (24°) and E-dipping detachment fault. At first sight, this finding seems to
838 confirm previous models on the 1908 causative fault that predict rupture along a low-angle and E-
839 dipping fault (e.g. Boschi et al., 1989; Valensise and Pantosti, 1992; Convertito and Pino, 2014;
840 Amoruso et al., 2002). Nevertheless, considering its dip-angle and the calculated overburden pressure
841 (320 Mpa, see section 6), stress analysis suggests the low-angle discontinuity as an almost
842 mechanically stable plane according to a typical angle of internal friction (φ) of 30° for brittle rocks.
843 A possible movement on such low-angle plane can therefore be postulated only for values of the
844 internal friction (φ) lower than 26° (Fig. 12 A). Such a low value accounts however for a mechanical
845 weakness of the low-angle discontinuity where stick-slip behaviour and the nucleation of large
846 earthquakes are unlikely (see Collettini et al., 2009; 2011). The current high strain rate (120 nano-
847 strain/yr) calculated for the Strait of Messina region (Mattia et al., 2009; Serpelloni et al., 2010) rather
848 suggest an almost aseismic stable-sliding motion of the low-angle discontinuity that produces large
849 interseismic strain in the area. Considering this scenario as unchanged in the last 100 years, nucleation
850 of large earthquakes on the low-angle discontinuity is unexpected, weakening therefore the previous
851 hypothesis on this issue. The inversion of geodetic data by using multiple sources (see section 6.1.2)
852 also suggests a less than primary role of the W-dipping faults occurring in southern Calabria in

853 generating large earthquakes. Though a seismic activation is predicted by the modelling for the Armo
854 Fault, the resolved normal dip-slip dislocation of 0.028m accounts however for a M<6 seismic event.
855 A sub-event, recorded in the seismogram five minutes after the 1908 mainshock (Oddone,1909),
856 could be attributed to a possible coseismic slip along the Armo fault. This inference is also suggested
857 by CSC analysis, where simulated displacement for an M~7 earthquake along the W-Fault can
858 transfer a dip-slip component of ~50 bar in the deeper portion of the Armo fault plane (see Fig. 13
859 H). Maximum uplift of 0.13 m at the footwall block of the Armo fault is apparently in contrast with
860 a possible low-magnitude event along this structure. However, the uplift magnitude in the area is also
861 best explained by a dip-slip movement on the low-angle discontinuity (see Fig. 13 A).
862
863 ## 8. Conclusion
864 Sub-seafloor geophysical explorations with unprecedented resolution provide new constraints on the
865 structural architecture and the seismotectonics of the Strait of Messina, the most seismically
866 hazardous region of Italy. Quaternary stretching in the area has been accommodated by the
867 development of an array of extensional faults occurring in the shallowest crustal portion of the
868 investigated area. Evidence for recent faulting is more apparent in the Sicilian side of the Strait where
869 the NNE-SSW trending W-Fault has displaced the seafloor by ~ 80 m about 3 km off the Sicilian
870 coast. The W-Fault emerges at the seafloor along the most rectilinear segment of the Messina Canyon
871 and right where previous authors observed/mapped triangular facets and suspended incisions (see
872 Ridente et al., 2014). Continuation across the southern Calabria mainland of the W-Fault has been
873 demonstrated by tilted-to-displaced Quaternary marine terraces along the Catona River valley,
874 accounting therefore for a total length of the fault of ~34.5 km (Fig. 15). A seismicity cut-off
875 evidenced by the high-precision relocated hypocentres in the area, suggests the occurrence of a
876 rheological boundary within the crustal depth roughly delineating a low-angle and E-dipping
877 discontinuity. V_p tomographic models enabled us to image the subcrustal setting of the investigated
878 sector revealing a large lithospheric doming in the upper plate of the Ionian Subduction Zone. The

879 upper plate doming localizes right where the slab is steepest, suggesting it is the result of supra-
880 subduction mantle wedging at subduction zone compensating slab retreat dynamics (Doglioni et al.,
881 1999; Gvirtzman and Nur, 1999; Faccenna et al., 2011). The large-scale folding of the upper plate
882 block is probably the main process controlling deformation in the area such as the uplift of the
883 Peloritani Mts. of Sicily and collapse to the east according to its asymmetry. The current large
884 interseismic strain rate in the area (Mattia et al., 2009; Serpelloni et al., 2010), along with the seismic
885 discontinuity and mechanical modelling, strongly suggest that collapse to the east of the lithospheric
886 doming (i.e. in the Strait of Messina area, see Fig. 11) is accommodated almost aseismically by the
887 low-angle, foreland-dipping discontinuity. In this framework and following the 3D-modeling, a
888 cause-and-effect relation between the mantle wedging/lithospheric bulging, sliding of the low-angle
889 fault, and the opening of the Strait of Messina can be invoked. Accordingly, Quaternary deformation
890 in the area and related seismotectonic processes are interpreted as the upper crustal response of a sub-
891 crustal process dominated by differential slab retreating and associated fore-arc mantle upwelling,
892 confirming previous studies in the area (Doglioni et al., 1999; Gvirtzman and Nur, 1999; Faccenna et
893 al., 2011). Alternatively, assuming a slab stalling in the area (Faccenna et al., 2001; Goes et al., 2004),
894 the localized mantle upwelling could be also explained by a consequence of crustal thinning along
895 the horsetail (or wing structure) termination of the Ionian Fault (Sgroi et al., 2021). A significant
896 reduction of the intermediate stress (sigma 3) could also provide stress perturbation and fault
897 triggering in the area (see Sgroi et al., 2021).
898 Finally, new data and analysis pointed to hierarchically different structural discontinuities with
899 distinct frictional behaviour that may have interacted with each other to produce large earthquakes in
900 the Strait of Messina region. The alternative deformation model proposed here is supported by the
901 CSC analysis and by the new inversion of the levelling data performed using multiple sources. The
902 two-independent analyses highlight that additional stress can be transferred mainly to the W-Fault
903 according to a simulated normal slip on the low-angle discontinuity and that an excellent fit between
904 calculated and observed subsidence is resolved by activating only the foreland-dipping fault and the

W-Fault. This confirms the significant role of the two discontinuities in producing subsidence in the area, whose cumulated effects can explain long, and short wavelength signals evidenced by the levelling pattern. To conclude, the W-fault along the axis of the Strait (and its extension in the Calabria onshore) is therefore proposed as the source of the 1908 earthquake, even though a coeval reactivation of the antithetic Armo fault in the Calabria mainland cannot be ruled out. Finally, results and interpretation coming from this paper, and particularly data concerning seismogenic faulting in the area, may be of significant interest for the design of the "Strait of Messina Bridge", planned many times in recent decades (see Fig. 15 for one of the planned bridge routes).

Acknowledgements

The Editor Gillian R. Foulger, Andrea Billi and an anonymous reviewer are warmly acknowledged for their constructive comments and suggestions that substantially improved the quality of the manuscript.
This work benefits from funding from the University of Catania in the frame of the project "Multidisciplinary analysis of the deformation around active tectonic structures" (supervisor G. Barreca) and was performed in the frame of the MUSE 4D project - Overtime tectonic, dynamic and rheologic control on destructive multiple seismic events -Special Italian Faults & Earthquakes: from real 4D cases to models in the frame of PRIN 2017. The authors acknowledge the use of MOVE Software Suite granted by Petroleum Experts Limited (www.petex.com). F. Cannavò from INGV-OE Catania is also acknowledged for the fruitful discussion on levelling data inversion through the GAME tool.

Figure Captions

Fig. 1 - The Strait of Messina in the tectonic framework of central Mediterranean. a) Location of the Calabrian Arc (CA) in the broader context of a collisional belt resulting from the convergence dynamics between the European Plate in the north and the African Plate in the south. b) Seismotectonics of the central Mediterranean area including the Calabrian Arc and the Eastern Sicily margin with draped the major Quaternary faults reported by previous authors (see Barreca et al. 2014, 2019; Cultrera et al., 2016, 2017; Billi et al., 2006; Gutscher et al. 2016) and strong (M>5) earthquakes (Pondrelli et al., 2006; Anderson and Jackson, 1987; Gasparini et al., 1982; Dziewonski et al., 1987). Blue contours represent the depth of the Ionian subduction interface (see Maesano et al., 2017). c) Location of the Strait of Messina in the fore-arc region of the Ionian Subduction Zone (ISZ). The subduction interface is modelled from the contours-data provided in Maesano et al., (2017). d) Quaternary faults (barbed on the downthrown side) slicing across the Strait of Messina area (see Ghisetti 1992; Monaco and Tortorici, 2000; Jacques et al., 2001; Argnani et al., 2009) and epicentre location and focal solution of the 1908 seismic event. Blue arrows represent space geodetic data in the Nubia reference frame (see Serpelloni et al.,2010). ARF, Armo Fault; CF, Cittanova Fault; MGF, Motta San Giovanni Fault; RCF, Reggio Calabria Fault; SCF, Southern Calabria Fault; SEF, S. Eufemia Fault; SF, Scilla Fault. Bathymetric data and topography were extracted from the Emodnet

bathymetry (http://www.emodnet-bathymetry.eu) and from the SRTM (Shuttle Radar Topography Mission) 30 plus topography (http://topex.ucsd.edu/WWW_html/srtm30_plus.html), respectively.

Fig. 2 – a) Macroseismic intensity field derived from the 1908 seismic event (from Baratta, 1910). b) Available levelling data from Loperfido (1909) are reported as blue (subsidence) and red (uplift) circles. Vertical change values are reported in supplementary Tab. I. c) Damage distribution of the December 1908 earthquake (data from Baratta 1910; Boschi et al., 1995; Monaco and Tortorici, 2007). Blue circles represent reported ground fracturing (see Blumetti et al., 2008). d) Previous models on the causative fault of the 1908 seismic event (view from the south).

Fig. 3 – a) Location of seismic grid in the offshore and framed in the on-land geological framework of the Strait of Messina (data from Lentini et al., 2000 – Sicilian side; Ghisetti, 1981; and http://geoportale.regione.calabria.it/opendata - Calabrian side). c) Location of drill-holes data and reconstructed stratigraphy (d) in the Strait of Messina offshore (data from Monaco et al., 1996). e) Trace location throught the available V_p models by Scarfì et al., (2018) and selected earthquakes in the 3D view (f).

Fig. 4 – a) Seismic facies analysis performed on the P204 seismic line crossing the Strait from Messina (in the NW) to Reggio Calabria (in the SE) and the interpreted seismo-stratigraphic model (b). Formational nomenclature according to Servizio Geologico d'Italia, 2007.

Fig. 5 – Tectonic interpretation over the P204, P1002, and P217 seismic lines showing previous compression overprinted by extensional tectonics. a) NW-dipping ramp-thrusts and associated anticlines and thrust-top basins interpreted along the P204 line and deforming the Mio-Pliocene sediment section. b) Thrust-top-basins along the P217 seismic line. c) The Pleistocene extensional W-Fault and associated minor structures observed along the P204 and P1002 (d) lines, respectively. Zooms on the bottom-right display the seafloor displacement (~80m) produced by Holocene activity of the W-Fault. m: multiple.

Fig. 6 - Morphotectonic map of the Catona River drainage basin in the northern mainland sector of the Strait of Messina, showing the altitude distribution of the Quaternary alluvial-marine terraces occurring in the area and fluvial deflection involving the Funica and Passo dei Limbi fluvial incisions. Dating of marine terraces are from Monaco et al. (2017) and reference therein. The dashed blue line indicates the location of the inferred tectonic structure that has been interpreted as the continuation on land of the W-Fault (see Fig. 7 for explanation). The red dashed lines are previous faults mapped in the area. Digital topographic data are from Regione Calabria (http://geoportale.regione.calabria.it/opendata)

Fig. 7 – Geological cross-section across the Catona River drainage basin (see Fig. 6 for profile trace locations) constrained by the re-mapped bottom boundaries of marine terraces of different ages. Geological profiling shows a miscorrelation between the terraces of the same aged located in the northern and southern flanks of the Catona River, strongly suggesting the occurrence of a tectonic structure in-between.

Fig. 8 – a) Map-view distribution of the relocated seismicity ($0.6<M<4.3$) recorded in the Strait of Messina region in the last 40 years (1981-2018) and available focal solutions (see Scarfì et al., 2020 and reference therein). b) Seismicity cut-off evidenced by the 3D-positioning of earthquakes in the crustal domain. c) Crustal section across the Strait of Messina interpreted following the seismicity distribution at depth (buffer of ± 17.5 km from the section trace) and nodal planes attitude (in section view) selected from available focal solutions. d) Stress tensor model for the investigated sector as

achieved by the inversion of the selected fault planes solutions (see dashed orange polygon in Fig. 8A) within a depth of 30 km. Earthquakes with (*) have hypocentral depth > 30 km and hence are not considered for stress inversion. The 1908 focal solution is from Gasperini et al. (1982).

Fig. 9 – a) Traces of vertical sections through the available V_p model (see Scarfì et al., 2018 and suppl. Fig. 5 for the uninterpreted lithospheric sections). c) V_p section B-B' selected for tectonic interpretation. Black dots are the earthquakes projected to the V_p section showing the position of the seismic discontinuity in the upper portion of the crust. d) Tectonic interpretation over the B-B' V_p section showing the architecture of the Ionian Subduction Zone (ISZ) and the upper plate doming occurring beneath the Peloritani Mts. in Sicily. The cut-off of seismicity, interpreted as a low-angle foreland-dipping discontinuity, occurs at the E-facing and steepest limb of the lithospheric culmination. d) Crustal section across the central Apennines used as analogue to interpret the Strait of Messina sub-crustal setting (see Barchi et al., 1998).

Fig. 10 – 3D modelling of the shallow (a) and deep-seated (b) structural discontinuities analysed in the present study. c) The subcrustal setting as achieved from the modelling of the Tyrrhenian Moho and of the Ionian slab showing the position of the upper plate doming.

Fig. 11 – a) Crustal to subcrustal 3D modelling of the study area (view from the NW) showing the position and the spatial relationships between the shallow faults (W-Fault, Armo, and Reggio Calabria faults) with the low-angle discontinuity, and location of the latter with respect to the upper plate doming. b) Cartoon (not-in-scale) explaining the possible significance of the low-angle discontinuity. Following the tectonic setting of the area, it has been interpreted as being an old decollement tilted by the upper plate doming.

Fig. 12 – a) Stress analysis performed over the low-angle discontinuity to evaluate its possible slip for different mechanical properties at the fault core. Using a typical angle of internal friction (φ) of 30° (inset 1), the discontinuity results stable whereas movement is allowed for angle of internal friction <26° (inset 2). b) Computed slip-tendency (average value = 0.38) for the low-angle discontinuity assuming a φ =30°. c) Comparison between the N-S width of the low-angle discontinuity with the subsidence measured after the 1908 seismic event in southern Calabria.

Fig. 13 – a) Predicted subsidence in the Strait of Messina topography as achieved from a simulated normal slip on the low-angle discontinuity. b) 3D geometries and nearby relationships between the Low-angle and overlying faults used as reference features to perform Coulomb Stress Change (CSC) analysis. Induced stress on the receiver W-Fault (c) and on the Armo fault (d) by stress perturbation caused by a normal slip on the low-angle discontinuity (source fault). e-g) Slip components of the induced CSC for the W-Fault. h-l) Components of induced stress on the Armo fault (receiver fault) by stress perturbation caused by a ~5 m of normal slip simulated on the W-Fault (source fault).

Fig. 14 – a) Generalized fault-planes exploited as dislocation sources for the inversion of levelling data. Black dots represent the benchmarks measured by Loperfido, (1909). Values of ground elevation changes are reported in supplementary Table II. b) Analytical inversion of the levelling data by using multiple sources showing a comparison between the recorded ground variations and the calculated. The best fit (red line) is achieved by the software computation by dislocating mainly the low-angle discontinuity and the W-Fault (see Table I).

Table 1 - Model parameters and related uncertainties resulting from levelling data inversion. Normal and left-lateral dislocation components are positive. The depth of the sources is referred to the sea level.

Fig. 15 – The W-Fault as mapped from seismic data interpretation and morphostructural analysis performed in southern Calabria overlapped with damage distribution (red polygons, Baratta, 1910) and ground fracturing (empty black circles, Blumetti et al., 2008) related to the 1908 seismic event. Blue dashed line is a telephone cable broken during the 1908 seismic event. The yellow star is the epicentre of the Messina-Reggio Calabria earthquake and related focal solution (Gasperini et al. 1982). Bathymetric data are from the M86/2 dataset (R/V Meteor).

References

Aki, K. and Richards, P. (1980) Quantitative Seismology. Theory and Methods. Freeman, San Francisco.

Anderson, H., Jackson, J.A., 1987. Deep seismicity of the Tyrrhenian Sea. Geophys. J.R. Astron. Soc. 91, 613–637.

Amodio-Morelli, L., Bonardi, G., Colonna, V., Dietrich, D., Giunta, G., Ippolito, F., et al., 1976. L'Arco Calabro-Peloritano nell'orogene Appenninico-Maghrebide. Mem. Soc. Geol. Ital. 17, 1–60.

Aloisi, M., Bruno, V., Cannavò, F., Ferranti, L., Mattia, M., Monaco, C. and M. Palano, M., 2013. Are the source models of the M 7.1 1908 Strait of Messinaearthquake reliable? Insights from a novel inversion and a sensitivity analysis of leveling data. Geophysical Journal International, 192, 3, 1025-1041, doi: 10.1093/gji/ggs062.

Amoruso, A., Crescentini, L., Scarpa, R., 2002. Source parameters of the 1908 Messina Straits, Italy, earthquake from geodetic and seismic data, J. geophys. Res., 107, doi:10.1029/2001JB000434.

Anderlini, L., Serpelloni, E., Belardinelli, M. E., 2016. Creep and locking of a low-angle normal fault: Insights from the Altotiberina fault in the Northern Apennines (Italy). Geophysical Research Letters, 43(9), 4321–4329. https://doi.org/10.1002/2016GL068604

Anderson, E. M., 1951. The Dynamics of Faulting, 2nd edition, Oliver and Boyd, Edinburgh, p. 206, 1951

Anderson, G., Johnson, H., 1999. A new statistical test for static stress triggering: application to the 1987 Superstition Hills earthquake sequence. J. Geophys. Res. 104: 20153–20168. http://dx.doi.org/10.1029/1999JB900200.

Antonioli, F., Ferranti, L., Lambeck, K., Kershaw, S., Verrubbi, V., Dai Pra, G., 2006. Late Pleistocene to Holocene record of changing upliftrates in southern Calabria and north-eastern Sicily (southern Italy, Central Mediterranean Sea), Tectonophysics, 422, 23–40.

Argnani A., Brancolini, G., Bonazzi, C., Rovere, M., Accaino, F., Zgur, F., Lodolo E., 2009. The result of the Taormina 2006 seismic survey: possible implications for active tectonics in the Messina Straits, Tectonophysics, 476, 159-169.

Axen, J.G., 1999. Low-angle normal fault earthquakes and triggering. Geophysical Research Letters, Vol. 26, No. 24, Pages 3693-3696, December 15, 1999

Balescu, S., Dumas, B., Guérémy, P., Lamothe, M., Lhénaff, R. Raffy, J., 1997- Thermoluminescence dating tests of Pleistocene sediments from uplifted marine shorelines along the southwest coastline of the Calabria Peninsula (southern Italy). Palaeog. Palaeocl. Palaeoecol., 130, 25-41.

Baratta, M., 1910. La catastrofe sismica calabro-messinese 28 dicembre 1908, relazione, Soc. Geogr. It., Rome.

Barbano, M.S., Azzaro, R., Grasso D. E., 2005. Earthquake damage scenarios and seismic hazard of messina, north-eastern sicily (italy) as inferred from historical data, journal of earthquake engineering, 9:6, 805-830, doi: 10.1080/13632460509350567

Barchi, M., Minelli, R., Pialli, G., 1998. The crop 03 profile: A synthesis of results on deep structures of the northern Apennines. Mem. Della Soc. Geol. Ital. 1998, 52, 383–400.

Barreca, G., Scarfì, L., Gross, F., Monaco, C., De Guidi, G., 2019. Fault pattern and seismotectonic potential at the south-western edge of the Ionian Subduction system (southern Italy): new field and geophysical constraints. Tectonophysics, Vol. 761 (2019) 31-45.

Barreca, G., Bruno, V., Cultrera, F., Mattia, M., Monaco, C., Scarfi, L., 2014. New insights in the geodynamics of the Lipari–Vulcano area (Aeolian Archipelago, southern Italy) from geological, geodetic and seismological data. J. Geodyn. 82 (2014), 150–167. https://doi.org/10.1016/j.jog.2014.07.003.

Barrier, P., 1986. Évolution paléogeographique du détroit de Messine au Pliocène et au Pléistocène. Giorn. di Geologia, 3, 48, 7-24.

Blumetti, A.M., Brustia, E., Comerci, V., Di Manna, P., Fiorenza, D., Guerrieri, L., Lucarini, M., Serva, L. Vittori E., 2008. The environmental effects of the 1908 southern Calabria—Messina earthquake (southern Italy), in Riassunti estesi delle comunicazioni Convegno GNGTS 2008, Trieste, pp. 202–206.

Billi, A., Barberi, G., Faccenna, C., Neri, G., Pepe, F., Sulli, A., 2006. Tectonics and seismicity of the Tindari Fault System, southern Italy: crustal deformations at the transition between ongoing contractional and exten-sional domains located above the edge of a subducting slab. Tectonics, 25, http://dx.doi.org/10.1029/2004TC001763.

Billi, A., Funiciello, R., Minelli, L., Faccenna, C., Neri, G., Orecchio, B., Presti, B., 2008. On the cause of the 1908 Messina tsunami, southern Italy. Geophysical Research Letters, Vol. 35, L06301, Doi:10.1029/2008gl033251, 2008

Billi, A., Minelli, L., Orecchio, D. & Presti, D. Constraints to the cause of three historical tsunamis (1908, 1783, and 1693) in the Messina Straits region, Sicily, southern Italy. *Seismol. Res. Lett.* **81**, 907–915. https ://doi.org/10.1785/gssrl .81.6.907 (2010).

Boncio, P., Brozzetti, F., Lavecchia, G., 2000. Architecture and seismotectonics of a regional low-angle normal fault zone in central Italy. Tectonics 2000, 19, 1038–1055.

Bonfiglio, L., Violanti D., 1983. Prima segnalazione di Tirreniano ed evoluzione pleistocenica di Capo Peloro (Sicilia nord-orientale). Geogr. Fis. Dinam. Quater., 6, 3-15.

Bonfiglio, L., 1972. Il Tirreniano di Bovetto e Ravagnese presso Reggio Calabria. Quaternaria, 16, 137-148.

Bonini, L., Di Bucci, D., Toscani, G., Seno, S., Valensise, G., 2011. Reconciling deep seismogenic and shallow active faults through analoguemodeling: the case of the Messina Straits (southern Italy), J. geol. Soc. Lond., 168, 191–199.

Boschi, E., Pantosti, D., Valensise, G., 1989. Modello di sorgente per il terremoto di Messina del 1908 ed evoluzione recente dell'area dello Stretto, Atti VIII Convegno G.N.G.T.S., Roma, 245-258.

Bottari, A., 2008. Osservazioni macrosismiche e studi, in Riassunti estesi del Convegno 1908–2008 Scienza e Societ`a a cento anni dal Grande Terremoto, Reggio Calabria 10–12 dicembre 2008, Miscellanea I.N.G.V., 3, pp. 19–20.

Bottari, A., Carapezza, E., Carapezza, M., Carveni, P., Cefali, F., Lo Giudice, E., Pandolfo C., 1986. The 1908 Messina Strait earthquake in the regional geostructural framework, Journal of Geodynamics, 5, 275-302.

Byerlee, J. D., 1978. Friction of rocks. Pure Appl. Geophys. 116, 615–629 (1978)
Cannavò, F., 2019. A new user-friendly tool for rapid modelling of ground deformation. Computers & Geosciences, 128, 60–69. https://doi.org/10.1016/j.cageo.2019.04.002

Capuano, P., De Natale, G., Gasparini, P., Pingue, F., Scarpa R., 1988. A model for the 1908 Messina Straits (Italy) earthquake by inversion of leveling data, Bull, Seismol. Soc. Am., 78, 1930-1947.

Caputo, M., 1979. Seismicity in the Straits of Messina, in L'attraversamento dello Stretto di Messina e la sua fattibilità, pp. 101–117, Atti dei Convegni Lincei, 43, Accademia Nazionale dei Lincei, Roma.

Colantoni, P., 1987. Marine geology of the Strait of Messina. Documents et Traveaux IGAL

Collettini, C., Niemeijer, A., Viti, C. et al. Fault zone fabric and fault weakness. Nature 462, 907–910 (2009). https://doi.org/10.1038/nature08585

Collettini, C. The mechanical paradox of low-angle normal faults: Current understanding and open questions. *Tectonophysics* **510,** 253–268 (2011).

Comerci, V., Vittori, E., Blumetti, A. M., Brustia, E., Di Manna, P., Guerrieri, L., Lucarini, M., Serva, L., 2015. Environmental effects of the December 28, 1908, Southern Calabria–Messina (Southern Italy) earthquake. Nat Hazards (2015) 76:1849–1891. DOI 10.1007/s11069-014-1573-x

Convertito, V. & Pino, N. A. Discriminating among distinct source models of the 1908 Strait of Messinaearthquake by modelling intensity data through full wavefield seismograms. *Geophysical Journal International* **198**, 164–173 (2014).

Cultrera, F., Barreca, G., Burrato, P., Ferranti, L., Monaco, C., Passaro, S., et al. 2016. Active faulting and continental slope instability in the Gulf of Patti (Tyrrhenian side of NE Sicily, Italy): A field,

marine and seismological joint analysis. *Natural Hazards*, *86* (April 2017), S253–S272. https://doi.org/10.1007/s11069-016-2547-y

Cultrera, F., Barreca, G., Ferranti, L., Monaco, C., Pepe, F., Passaro, S., et al. (2017). Structural architecture and active deformation pattern in the northern sector of the Aeolian-Tindari-Letojanni fault system (SE Tyrrhenian Sea-NE Sicily) from integrated analysis of field, marine geophysical, seismological and geodetic data. *Italian Journal of Geosciences*, *136*(3), 399–417. https://doi.org/10.3301/IJG.2016.17

D'Agostino, N., Selvaggi, G., 2004. Crustal motion along the Eurasia- Nubia plate boundary in the Calabrian Arc and Sicily and active extension in the Messina Straits of from GPS measurements, J. geophys. Res., 109(B11402), doi:10.1029/2004JB002998.

D'Agostino, N., D'Anastasio, E., Gervasi, A., Guerra, I., Nedimovi´c, M.R., Seeber, L., Steckler, M., 2011. Forearc extension and slow rollback of the Calabrian Arc from GPS measurements, Geophys. Res. Lett., 38(L17304), doi:10.1029/2011GL048270.

De Guidi, G., Catalano, S., Monaco, C., Tortorici, L., 2003. Morphological evidence of Holocene coseismic deformation in the Taormina region (NE Sicily). J. Geodyn. 36, 193–211.

De Natale, G., Pingue, F., 1991. A variable slip fault model for the 1908 Messina Straits (Italy) earthquake, by inversion of leveling data, Geophys. J. Int., 104, 73-84, 1991

Del Ben, A., Gargano, C., Lentini, F., 1996. Ricostruzione strutturale e stratigrafica dell'area dello Stretto di Messina mediante analisi comparata dei dati geologici e sismici. Mem. Soc. Geol. Ital., 51, 703-717.

Di Stefano, A., Longhitano, S.G., 2009. Tectonics and sedimentation of the Lower and Middle Pleistocene mixed siliciclastic/bioclastic sedimentary successions of the Ionian Peloritani Mts (NE Sicily, Southern Italy): the onset of opening of the Messina Strait. Central Eur. Journ. Of Geosciences, 1(1), 33-62.

Doglioni, C., Ligi, M., Scrocca, D., Bigi, S., Bortoluzzi, G., Carminati, E., Cuffaro, M., D'Oriano, F., Forleo, V., Muccini, F., Riguzzi, F., 2012. The tectonic puzzle of the Messina area (Southern Italy): Insights from new seismic reflection data. Scientific Reports 2, 970 (2012).

Doglioni, C., Carminati, E., Petricca, P., Riguzzi, F., 2005. Normal fault earthquakes or Graviquakes. Scientific Reports | 5:12110 | DOI: 10.1038/srep12110

Doglioni, C., Harabaglia, P., Merlini, S., Mongelli, F., Peccerillo, A., Piromallo, C., 1999. Orogens and slabs vs their direction of subduction. Earth Science Reviews, 45, 167–208.

Doglioni, C., Innocenti, F. Mariotti, G., 2001. Why Mt Etna? Terra Nova, 13, 25–31.

Doglioni, C., Tonarini, S., Innocenti, F., 2009. Mantle wedge asymmetries along opposite subduction zones. Lithos, 113, 179e189. https://doi.org/10.1016/j.lithos.2009.01.012

Dumas, B., Gueremy, P., Lhenaff, R., Raffy J., 1982. Le soulèvement quaternaire de la Calabre méridionale. Revue de Géol. Dynam. et de Géogr. Physique, 23, 27-40.

Dziewonski, A.M., Ekström, G., Franzen, J.E., Woodhouse, J.H., 1987. Global seismicityof 1978: centroid-moment tensor solutions for 512 earthquakes. Phys. EarthPlanet. Inter. 46, 316–342.

Faccenna, C., Becker, T. W., Auer, L., Billi, A., Boschi, L., Brun, J-P., Capitanio, F. A., Funiciello, F., Horvath, F., Jolivet, L., Piromallo, C., Royden, L., Rossetti, F., Serpelloni, E., 2014. Mantle dynamics in the Mediterranean. *Reviews of Geophysics*, *52*(3), 283 - 332. https://doi.org/10.1002/2013RG000444

Faccenna, C., Piromallo, C., Crespo-Blanc, A., Jolivet, L., Rossetti, F., 2004. Lateral slab deformation and the origin of western Mediterranean arcs, Tectonics, 23, TC1012, doi:10.1029/2002TC001488.

Faccenna, C., Becker, T. W., Lucente, F., Jolivet, L., Rossetti, F. 2001. History of subduction and back-arc extension in the central Mediterranean, Geophys. J. Int., 145, 809–820, doi:10.1046/j.0956-540x.2001.01435.x.

Ferranti, L., Monaco, C., Antonioli, F., Maschio, L. Morelli, D., 2008. Holocene activity of the Scilla fault, southern Calabria: insights from morpho-structural and marine geophysical data. Tectono-physics, 453, 74-93.

Ferranti, L., Monaco, C., Morell,i D., Tonielli, R. Tortorici, L., Badalini, M., 2008. Morphostructural setting and active faults in the Messina Strait: new evidence from marine geological data. Rend. Online Soc. Geol. It., 1, 86-88

Ferranti, L., Monaco, C., Antonioli, F., Maschio, L., Kershaw, S., Verrubbi, V., 2007. The contribution of regional uplift and coseismic slip to the vertical crustal motion in the Messina Straits, Southern Italy: evidence from raised Late Holocene shorelines, J. geophys. Res., 112(B06401), doi:10.1029/2006JB004473.

Gasparini, C., Iannacone, G., Scandone, P., Scarpa, R., 1982. Seismotectonics of the Calabrian Arc. Tectonophysics 82, 267–286.

Ghisetti, F., 1981. Upper Pliocene-Pleistocene uplift rates as indicators of neotectonic pattern: an example from southern Calabria (Italy). Zeitschrift für Geomorph., 40, 93-118

Ghisetti, F., Vezzani, L., 1982. Different styles of deformation in the Calabrian Arc (southern Italy): implications for a seismotectonic zoning, Tectonophysics, 85, 149–165

Ghisetti, F., 1984. Recent deformations and the seismogenic source in the Messina Straits (southern Italy), Tectonophysics, 109, 191–208.

Ghisetti, F., 1992. Fault parameters in the Messina Straits (southern Italy) and relations with the seismogenic source, Tectonophysics, 210, 117–133.

Goes, S., Giardini, D., Jenny, S., Hollenstein, C., Kahle, H.G., Geiger, A. 2004. A recent tetconic reorganization in the south-central Mediterranean, Earth Planet. Sci. Lett., 226, 335-345.

Gutscher, M.-A., Dominguez, S., Mercier de Lepinay, B., Pinheiro, L., Gallais, F., Babonneau, N., Cattaneo, A., Le Faou, Y., Barreca, G., Micallef, A., Rovere, M., 2016. Tectonic expression of an active slab tear from high-resolution seismic and bathymetric data offshore Sicily (Ionian Sea). Tectonics 34, 39–54. https://doi.org/10. 1002/2015TC003898.

Gvirtzman, Z., Nur, A.,1999. Plate detachment, asthenosphere upwelling, and topography across subduction zones. Geology; June 1999; v. 27; no. 6; p. 563–566; 4 figures.
Jacques, E., Monaco, C., Tapponnier, P., Tortorici, L., Winter, T., 2001. Faulting and earthquake triggering during the 1783 Calabria seismic sequence, Geophys. J. Int., 147, 499–516.

Jaeger, J. C., Cook, N. G. W., 1979. Fundamentals of Rock Mechanics. Springer Netherlands.

Jolivet, L., Faccenna, C., 2000. Mediterranean extension and the African-Eurasian collision, Tectonics, 19, 1095–1106, doi:10.1029/ 2000TC900018.

Johnston, S.T., Mazzoli, S., 2009. 'The Calabrian Orocline: buckling of a previously more linear orogen', Geological Society, London. Special Publications 327 (1), 113–125.

King, G.C.P., Stein, R.S., Lin, J., 1994. Static stress changes and the triggering of earthquakes. Bull. Seismol. Soc. Am. 84, 935–953

Lentini, F., 2000. Carta Geologica della Provincia di Messina, scala 1:50.000, 3 fogli, S.El.Ca., Firenze.

Leonard, M., 2010. Earthquake Fault Scaling: Self-Consistent Relating of Rupture Length, Width, Average Displacement, and Moment Release. Bulletin of the Seismological Society of America, vol. 100, issue 5A, pp. 1971-1988. Doi: 10.1785/0120090189

Loperfido, A., 1909. Livellazione geometrica di precisione eseguita dall'I.G.M. sulla costa orientale della Sicilia, da Messina a Catania, a Gesso ed a Faro Peloro e sulla costa occidentale della Calabria da Gioia Tauro a Melito di Porto Salvo, in Relazione della Commissione Reale incaricata di designare le zone più adatte per la ricostruzione degli abitati colpiti dal terremoto del 28 dicembre 1908 o da altri precedenti, pp.131–156, Accademia Nazionale dei Lincei, Roma.

Lund, B., Slunga, R., 1999. Stress tensor inversion using detailed microearthquake information and stability constraints: Application to Olfus in southwest Iceland, J. Geophys. Res. 104, 14.947-14.964.
Maesano, F.E., Tiberti, M.M., Basili, R., 2017. The Calabrian Arc: three dimensional modelling of the subduction interface. Scientific Reports | 7: 8887 | DOI:10.1038/s41598-017-09074-8

Malinverno, A., Ryan, W.B.F., 1986. Extension in the Tyrrhenian Sea and shortening in the Apennines as a result of arc migration driven by sinking of the lithosphere, Tectonics, 5, 227-245.

Mattia, M., Palano, M., Bruno,V., Cannavò, F., 2009. Crustal motion along the Calabro-Peloritano Arc as imaged by twelve years of measurements on a dense GPS network, *Tectonophysics,* **476,** 528–537.

Mercalli, G., 1909. Contributo allo studio del terremoto calabro-messinese del 28 dicembre 1908, Atti Ist. Incoraggiamento Napoli, 3, 1-46.

Meschis, M., Roberts, G. P., Mildon, Z. K., Robertson, J., Michetti, A. M., Faure Walker, J. P. 2019. Slip on a mapped normal fault for the 28th December 1908 Messina earthquake (Mw 7.1) in Italy. Scientific Reports, 9, 1–8. https://doi.org/10.1038/s41598-019-42915-2

Monaco, C., Barreca, G., Di Stefano, A., 2017. Quaternary marine terraces and fault activity in the northern mainland sectors of the Messina Strait (southern Italy). Italian Journal of Geosciences DOI: 10.3301/IJG.2016.10.

Monaco, C., Tortorici, L., 2007. Active faulting and related tsunami in eastern Sicily and south-western Calabria, Boll. Geofis. Teor. Appl., 48(2) 163–184.

Monaco, C., Tortorici, L., 2000. Active faulting in the Calabrian arc and eastern Sicily, J. Geodynamics, 29, 407-424.

Monaco, C., Tortorici, L., Cernobori, L., Nicolich, R., Costa, M., 1996. From collisional to rifted basins: an example from the southern Calabrian Arc (Italy), Tectonophysics, 266, 233-249.

Michael, A.J., 1984. Determination of stress from slip data: Faults and folds, *J. Geophys. Res*. **89**, 11.517-11.526.

Michael, A.J., 1987. Use of focal mechanisms to determine stress: A control study, *J. Geophys. Res*. **92**, 357-368.

Miyauchi, T., Dai Pra, G., SylosLabini S., 1994. Geochronology of Pleistocene marine terraces and regional tectonics in the Tyrrhenian coast of South Calabria, Italy. Il Quaternario, **7**, 17-34.

Mulargia, F., Boschi, E., 1983. The 1908 Messina earthquake and related seismicity, in Earthquakes: observation, theory and interpretation, edited by H. Kanamori and E. Boschi, Proc. Int. Sch. Phys. Enrico Fermi, Course LXXXV, 493-518.

Neri, G., Barberi, G., Orecchio, B., Mostaccio, A., 2003. Seismic strain and seismogenic stress regimes in the crust of the southern Tyrrhenian region. Earth and Planetary Science Letters, 213, 97–112.

Neri, G., Barberi, G., Oliva, G., Orecchio, B., 2004. Tectonic stress and seismogenic faulting in the area of the 1908 Messina earthquake, south Italy. Geophysical Research Letters, 31, L10602. https://doi.org/10.1029/2004GL1019742

Neri, G., Barberi, G., Oliva, G., Orecchio, B., 2005. Spatial variations of seismogenic stress orientations in Sicily, south Italy. Physics of the Earth and Planetary Interiors, 148, 175–191.

Oddone, E., 1909. Appunti fisici per lo studio del terremoto di Sicilia e Calabria. In: Annali della Soc degli Ing ed Arch Italiani, fasc 7. Roma

Ogniben, L., 1969. Schema introduttivo alla geologia del Confine calabro-lucano. Mem. Soc. Geol. Ital. 8, 453–763.

Omori, E., 1909. Preliminary report on the Messina-Reggio earthquake of Dec. 28, 1908, Bull. Imp. Earth. Comm., 3- 2, 37-46.

Patacca, E., Scandone P., 1989. Post Tortonian mountain building in the Apennines: The role of the passive sinking of a relict lithospheric slab, in The Lithosphere in Italy, vol. 80, edited by A. Boriani et al., pp. 157–176, Atti Conv. Lincei, Rome.

Pino, A., Piatanesi, A., Valensise, G., Boschi, E., 2009. The 28 December 1908 Messina Straits earthquake (Mw 7.1): a great earthquake throughout a century of seismology, Seismol. Res. Lett., 80(2), 243–259.

Pino, N.A., Giardini, D., Boschi, E., 2000. The December 28, 1908, Messina Straits, southern Italy, earthquake: waveform modeling of regional seismograms, J. geophys. Res., 105(B11), 25 473–25 492.

Platania, G., 1909. Il maremoto dello Stretto di Messina del 28 dicembre 1908, Boll. Soc. Sismol. It., 13, 369-458.

Pondrelli, S., Salimbeni, S., Ekström, G., Morelli, A., Gasperini, P., Vannucci, G., 2006.The Italian CMT dataset from 1977 to the present. Phys. Earth Planet. Inter. http://dx.doi.org/10.1016/j.pepi.2006.07.008, 159/3-4, 286–303.

Presti, D., Billi, A., Orecchio, B., Totaro, C., Faccenna, C., Neri, G., 2013. Earthquake focal mechanisms, seismogenic stress, and seismotectonics of the Calabrian Arc, Italy. Tectonophysics, 602, 153–175.

Rabbel, W., Kaban, M.K., Tesauro, M., 2013. Contrasts of seismic velocity, density and strength across the Moho. Tectonophysics 609, 437–455. https://doi.org/10.1016/j. tecto.2013.06.020.

Reasenberg, P. A., Simpson, R. W.,1992. Response of regional seismicity to the static stress change produced by the Loma Pietra earthquake. Science, 255, 1687-1690.

Rice, J. R., 1992 in Fault Mechanics and Transport Properties of Rocks (eds Evans, B. & Wong, T.-f.) 475–503 (Academic Press, 1992).

Ridente, D., Martorelli, E., Bosman, A., Chiocci, F. L.,2014. High-resolution morpho-bathymetric imaging of the Messina Strait (Southern Italy). New insights on the 1908 earthquake and tsunami. Geomorphology 208, 149–159 (2014).

Rovida, A., Locati, M., Camassi, R., Lolli, B., Gasperini, P., 2019. Catalogo Parametrico dei Terremoti Italiani (CPTI15), versione 2.0. Istituto Nazionale di Geofisica e Vulcanologia (INGV). https://doi.org/10.13127/CPTI/CPTI15.2

Scandone, P., 1979. Origin of the Tyrrhenian Sea and Calabrian Arc, Boll. Soc. Geol. Ital., 98, 27–34.

Scarfì, L., Langer, H., Scaltrito, A., 2009. Seismicity, seismotectonics and crustal velocity structure of the Messina Strait (Italy), Phys. Earth planet. Inter., 177, 65–78.

Scarfì, L., Messina, A., Cassisi, C., 2013. Sicily and southern Calabria focal mechanism database: A valuable tool for the local and regional stress field determination. Annals of Geophysics, 56, 1.

Scarfi, L., Barberi, G., Musumeci, C., Patane, D., 2016. Seismotectonics of northeastern Sicily and southern Calabria (Italy): New constraints on the tectonic structures featuring in a crucial sector for the central Mediterranean geodynamics. Tectonics 35, 812–832. https://doi.org/10.1002/2015TC004022 (2016).

Scarfì, L., Barberi, G., Barreca, G., Cannavo, F., Koulakov, I., Patane, D., 2018. Slab narrowing in the Central Mediterranean: the Calabro-Ionian subduction zone as imaged by high resolution seismic tomography. Sci. Rep. 2018 (8), 5178. https://doi. org/10.1038/s41598-018-23543-8.

Scarfì, L., Langer, H., Messina, A., Musumeci, C., 2020. Tectonic regimes inferred from clustering of focal mechanisms and their distribution in space: application to the Central Mediterranean Area. Journal of Geophysical Research: Solid Earth, 125, e2020JB020519. https://doi.org/10.1029/2020JB020519.

Spampinato, C.R., Braitenberg, C., Monaco, C., Scicchitano G., 2013. Analysis of vertical movements in eastern Sicily and southern Calabria (Italy) through geodetic levelling data. Journ. of Geodynamics, **66**, 1-12, http://dx.doi.org/10.1016/j.jog.2012.12.002.

Schick, R., 1977. Eine seismotektonische Bearbeitung des Erdbebens von Messina im Jahre 1908. Geologisches Jahrbuch, Reihe E 11, 74 pp.

Schambach, L. Grilli, S.T., Tappin, D.R., Gangemi, M.D., Barbaro, G., 2020. New simulations and understanding of the 1908 Messina tsunami for a dual seismic and deep submarine mass failure source. Marine Geology, 421 (2020) 106093. https://doi.org/10.1016/j.margeo.2019.106093.

Scicchitano, G., Lo Presti, V., Spampinato, C., Gasparo Morticelli, M., Antonioli, F., Auriemma, R., Ferranti L., Monaco, C., 2011. Millstones as indicators of relative sea-level changes in northern Sicily and southern Calabria coastlines, Italy. Quat. Intern., 232, 92-104, doi: 10.1016/jquaint.2010.08.019.

Serpelloni, E., 2014. Mantle dynamics in the Mediterranean. Rev. Geophys. 52, 283–332. https://doi.org/10.1002/2013RG000444.

Serpelloni, E., Bürgmann, R., Anzidei, M., Baldi, P., Mastrolembo, B., Boschi, E., 2010. Strain accumulation across the Messina Straits and kinematics of Sicily and Calabria from GPS data and dislocation modeling, Earth planet. Sci. Lett., 298(3–4), 347–360.

Servizio Geologico d'Italia, 2007. Foglio 601 Messina-Reggio di Calabria della Carta Geologica d'Italia alla scala 1:50.000. (ISPRA).

Sibson, R. H., 1985. A note on fault reactivation, J. Struct. Geol., 7, 751– 754.

Stein, R.S., 1999. The role of stress transfer in earthquake occurrence. Nature 402: 605–609. http://dx.doi.org/10.1038/45144.

Sgroi, T., Polonia, A., Barberi, G., Andrea Billi, A., Gasperini, L., 2021. New seismological data from the Calabrian arc reveal arc-orthogonal extension across the subduction zone. Scientific Reports | (2021) 11:473 | https://doi.org/10.1038/s41598-020-79719-8

Tortorici, L., Monaco, C., Tansi, C., Cocina, O., 1995. Recent and active tectonics in the Calabrian Arc (Southern Italy), Tectonophysics, 243, 37-49.

Totaro, C., Orecchio, B., Presti, D., Scolaro, S., Neri, G., 2016. Seismogenic stress field estimation in the Calabrian Arc region (south Italy) from a Bayesian approach. Geophysical Research Letters, 43, 8960–8969. https://doi.org/10.1002/2016GL070107

Valensise, G., Pantosti, D., 1992. A 125-Kyr-long geological record of seismic source repeatability: the Messina Straits (southern Italy) and the 1908 earthquake (MS $7^{1/2}$), Terra Nova, 4, 472-483.

Vannucci, G., Gasperini, P., 2003. A database of revised fault plane solutions for Italy and surrounding regions. Computers & Geosciences, 29, 903–909.

Wells, D.L., Coppersmith, K.J., 1994. New Empirical Relationships among Magnitude, Rupture Length, Rupture Width, Rupture Area, and Surface Displacement. Bulletin of the Seismological Society of America 84 (4), 974-1002.

Wernicke, B., 1981. Low-angle normal faults in the Basin and Range Province: nappe tectonics in an extending orogen. Nature volume 291, pages645–648(1981)

Westaway, R., 1992. Seismic moment summation for historical earthquakes in Italy: tectonic implications, J. geophys. Res., 97, 15 437–15 464.

Westaway, R., 1993. Quaternary uplift of Southern Italy, J. geophys. Res., 98, 21 741–21 722.

Wortel, M.J.R., Spakman, W., 2000. Subduction and slab detachment in the Mediterranean-Carpathian region, Science, 290, 1910–1917.

Vavryčuk, V., 2014. Iterative joint inversion for stress and fault orientations from focal mechanisms, *Geophysical Journal International*, **199**, 69-77, doi: 10.1093/gji/ggu224.

Zhang, H., Thurber, C. Bedrosian, P., 2009. Joint inversion for Vp, Vs, and Vp/Vs at SAFOD, Parkfield, California. Geochem. Geophys. Geosyst. 10(Q110032), https://doi.org/10.1029/2009GC002709 (2009).

Zoback, M. D., Zoback, M. L., Mount, V. S., Suppe, J., Eaton, J. P, Healy, J. H., Oppenheimer, D., Reasenberg, P., Jones, L., Raleigh, C. B., Wong, I. G., Scotti, O., Wentworth, C., 1987. New evidence on the state of stress of the San Andreas fault system. Science 238, 1105–1111 (1987)

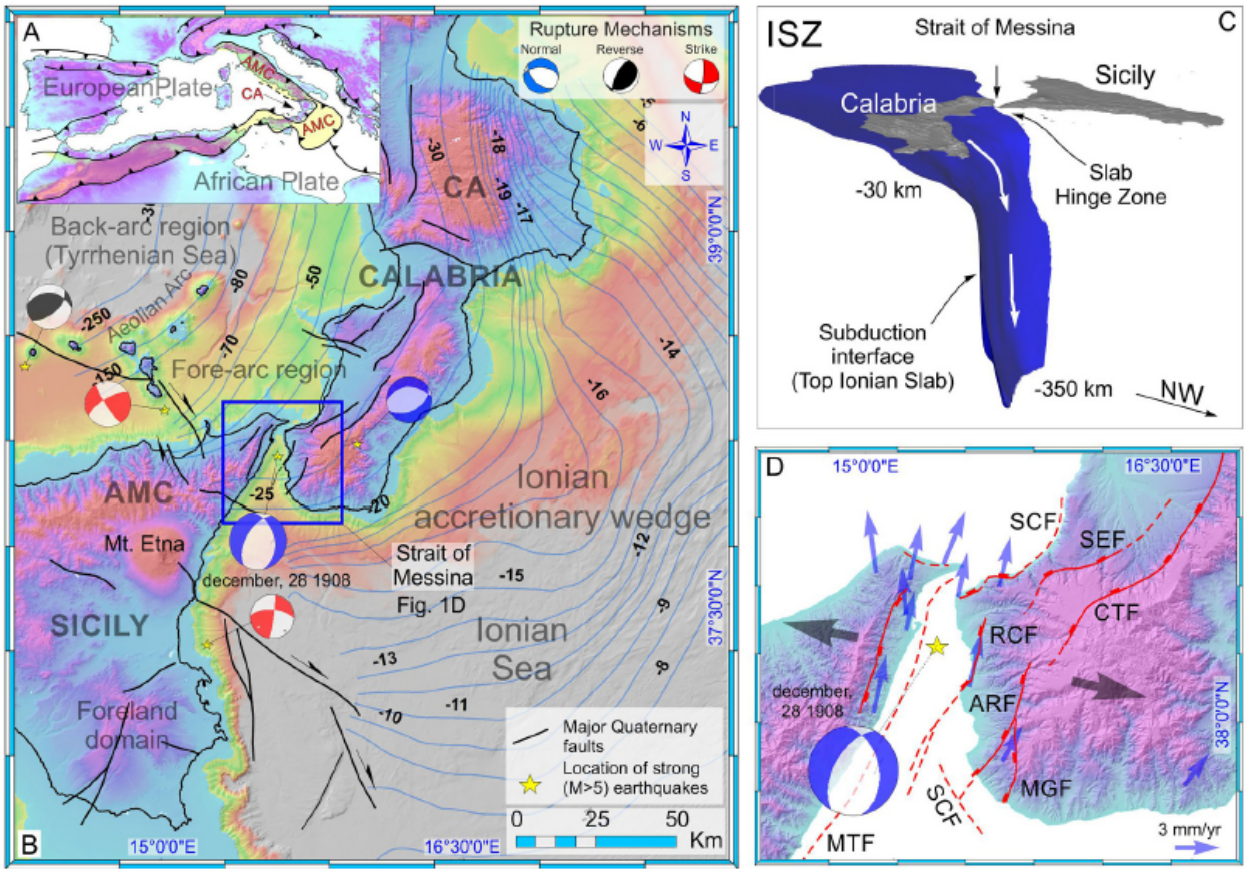
A
Rupture Mechanisms
Normal
Reverse
Strike
EuropeanPlate
African Plate
AMC
CA
Back-arc region
(Tyrrhenian Sea)
Aeolian Arc
Fore-arc region
CALABRIA
Ionian
accretionary wedge
Mt. Etna
AMC
SICILY
december, 28 1908
Strait of
Messina
Fig. 1D
Ionian
Sea
Foreland
domain
Major Quaternary
faults
Location of strong
(M>5) earthquakes
0 25 50 Km
B
15°0'0"E
16°30'0"E
39°0'0"N
37°30'0"N
ISZ
Strait of Messina
C
Calabria
Sicily
-30 km
Slab
Hinge Zone
Subduction
interface
(Top Ionian Slab)
-350 km
NW
D
15°0'0"E
16°30'0"E
SCF
SEF
CTF
RCF
ARF
MGF
SCF
MTF
december,
28 1908
38°0'0"N
3 mm/yr

Figure 1

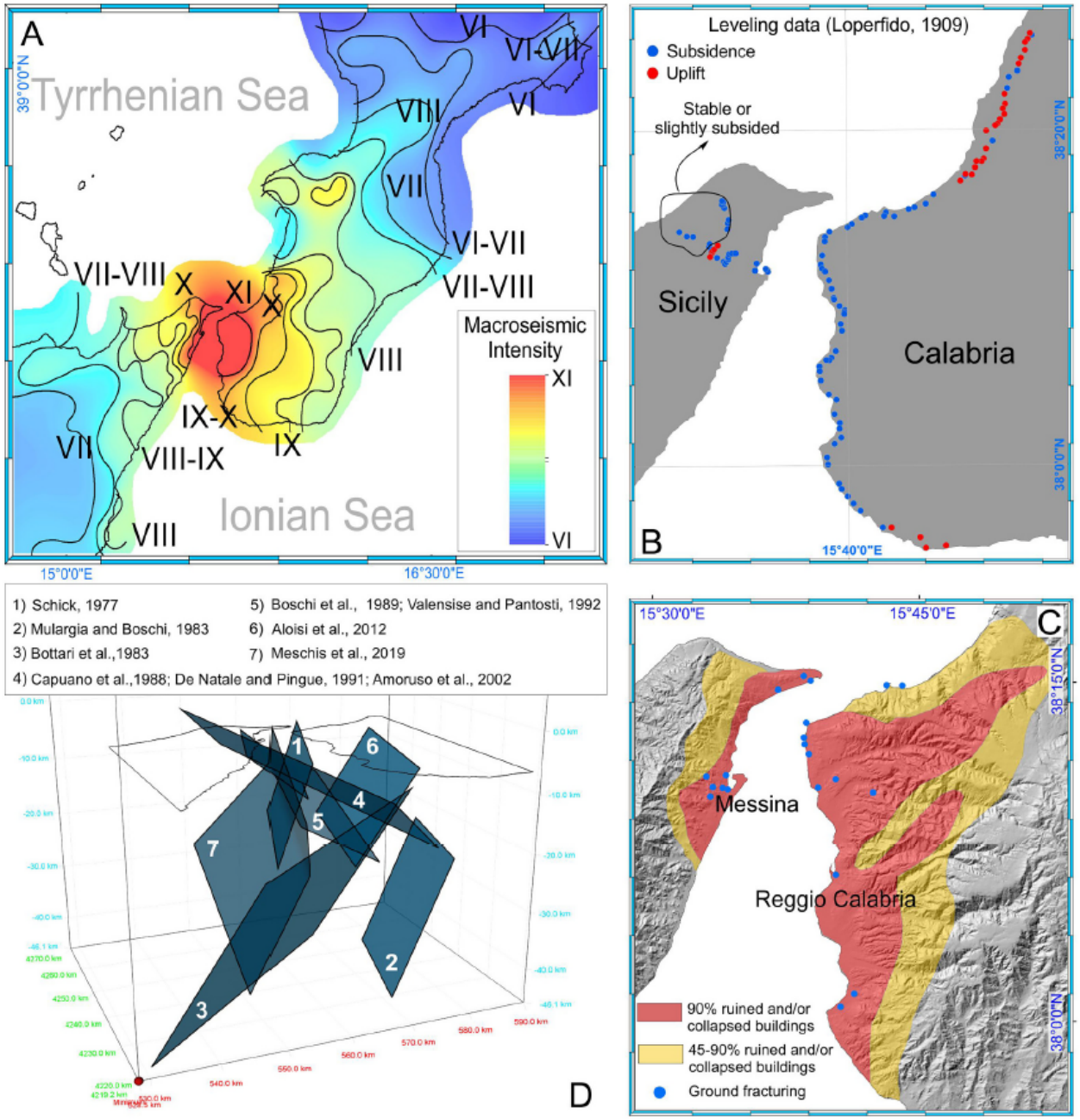
A
Tyrrhenian Sea
Ionian Sea
VI
VI-VII
VIII
VII
VII-VIII
X
XI
IX-X
IX
VIII-IX
Macroseismic Intensity
XI
VI
39°0'0"N
15°0'0"E
16°30'0"E
Leveling data (Loperfido, 1909)
Subsidence
Uplift
Stable or slightly subsided
Sicily
Calabria
38°20'0"N
38°0'0"N
15°40'0"E
B
1) Schick, 1977
2) Mulargia and Boschi, 1983
3) Bottari et al.,1983
4) Capuano et al.,1988; De Natale and Pingue, 1991; Amoruso et al., 2002
5) Boschi et al., 1989; Valensise and Pantosti, 1992
6) Aloisi et al., 2012
7) Meschis et al., 2019
D
15°30'0"E
15°45'0"E
C
Messina
Reggio Calabria
38°15'0"N
38°0'0"N
90% ruined and/or collapsed buildings
45-90% ruined and/or collapsed buildings
Ground fracturing

Figure 2

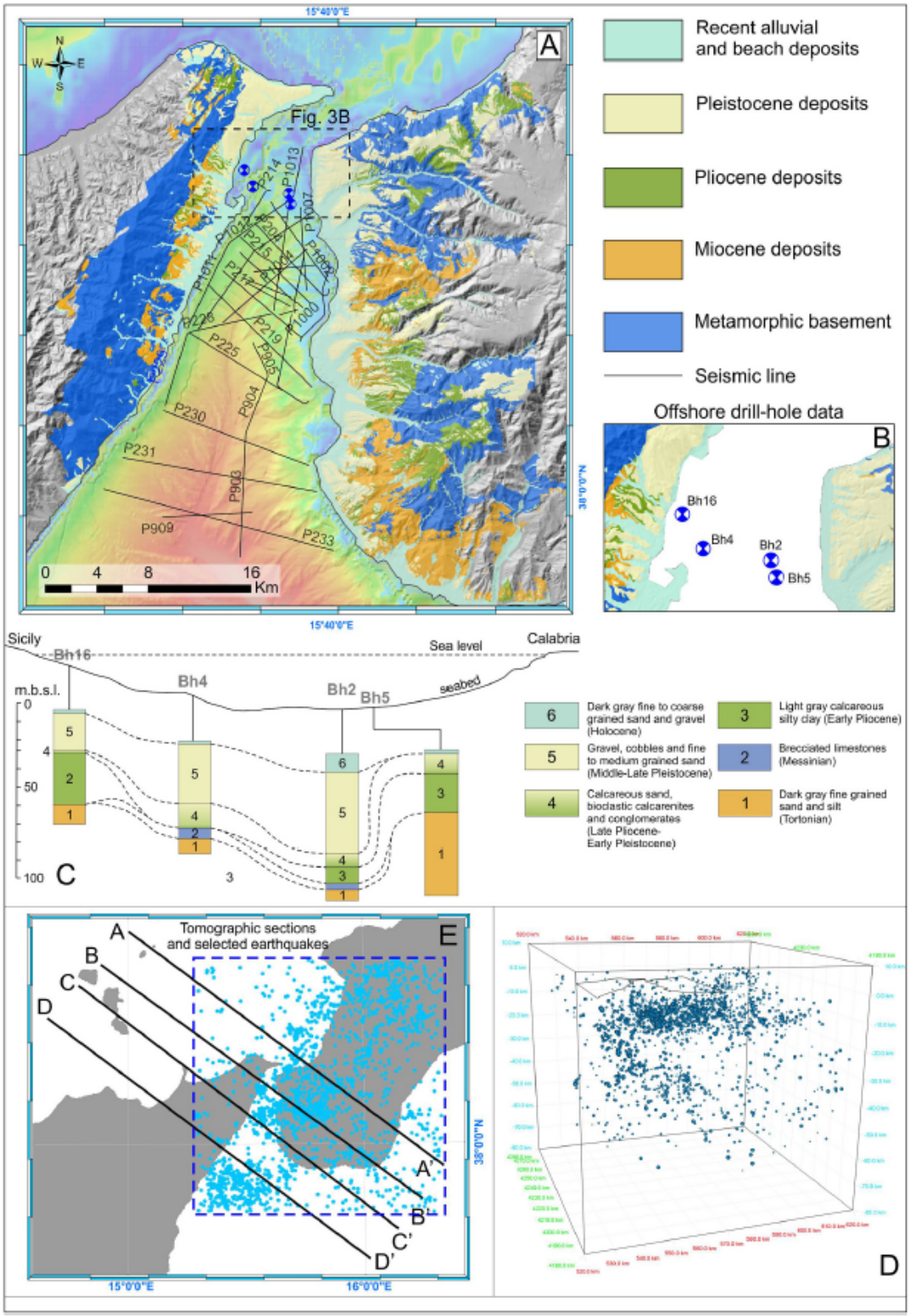
A
Fig. 3B
Recent alluvial and beach deposits
Pleistocene deposits
Pliocene deposits
Miocene deposits
Metamorphic basement
Seismic line
Offshore drill-hole data
B
Bh16
Bh4
Bh2
Bh5
Sicily
Calabria
Sea level
seabed
m.b.s.l.
C
Dark gray fine to coarse grained sand and gravel (Holocene)
Gravel, cobbles and fine to medium grained sand (Middle-Late Pleistocene)
Calcareous sand, bioclastic calcarenites and conglomerates (Late Pliocene-Early Pleistocene)
Light gray calcareous silty clay (Early Pliocene)
Brecciated limestones (Messinian)
Dark gray fine grained sand and silt (Tortonian)
Tomographic sections and selected earthquakes
E
D
15°40'0"E
38°0'0"N
15°0'0"E
16°0'0"E

Figure 3

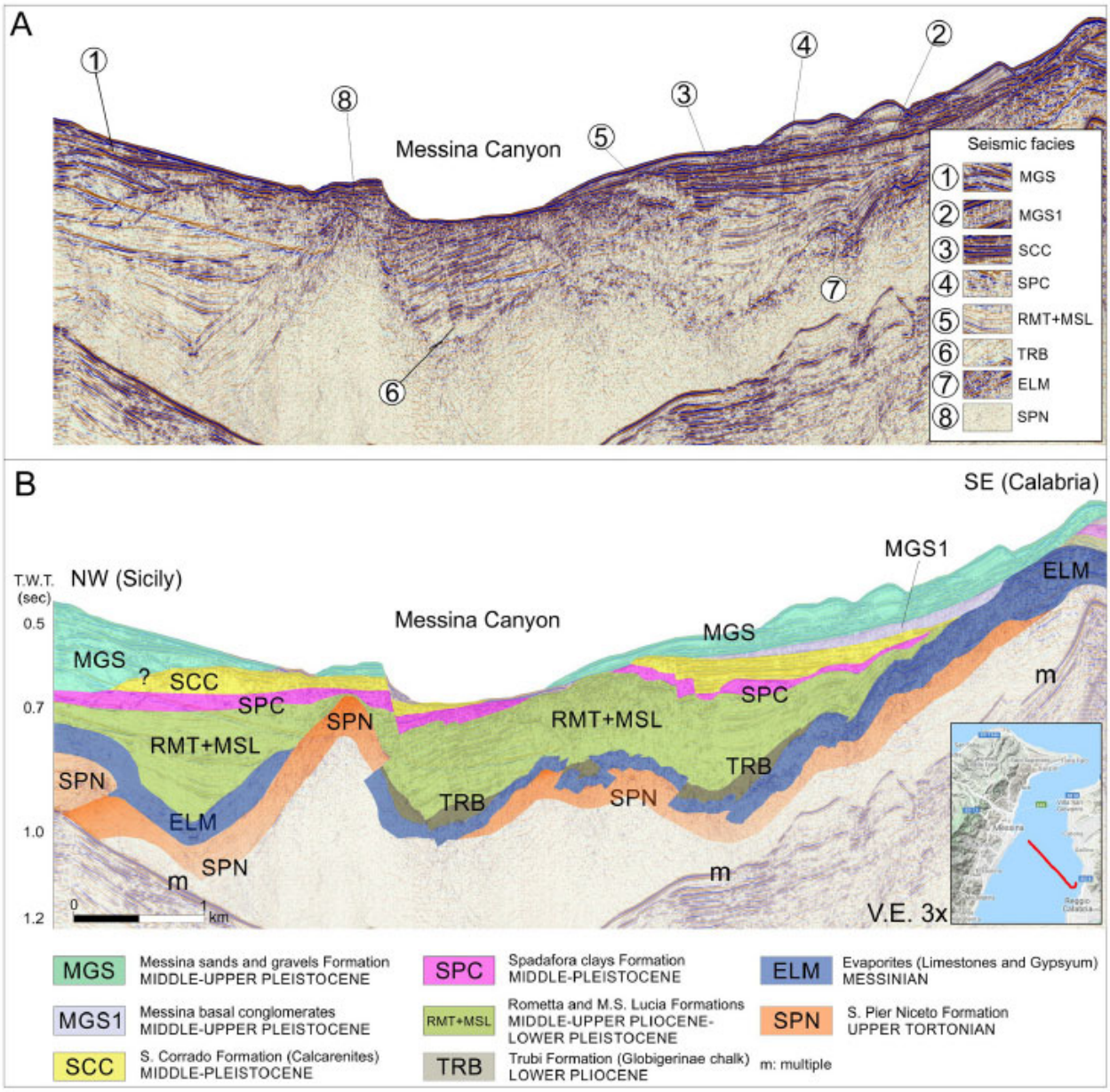
A
Messina Canyon
Seismic facies
MGS
MGS1
SCC
SPC
RMT+MSL
TRB
ELM
SPN
B
SE (Calabria)
NW (Sicily)
T.W.T. (sec)
0.5
0.7
1.0
1.2
Messina Canyon
MGS
MGS1
ELM
SCC
SPC
SPN
RMT+MSL
TRB
m
0
1
km
V.E. 3x
Messina sands and gravels Formation
MIDDLE-UPPER PLEISTOCENE
Messina basal conglomerates
MIDDLE-UPPER PLEISTOCENE
S. Corrado Formation (Calcarenites)
MIDDLE-PLEISTOCENE
Spadafora clays Formation
MIDDLE-PLEISTOCENE
Rometta and M.S. Lucia Formations
MIDDLE-UPPER PLIOCENE-
LOWER PLEISTOCENE
Trubi Formation (Globigerinae chalk)
LOWER PLIOCENE
Evaporites (Limestones and Gypsyum)
MESSINIAN
S. Pier Niceto Formation
UPPER TORTONIAN
m: multiple

Figure 4

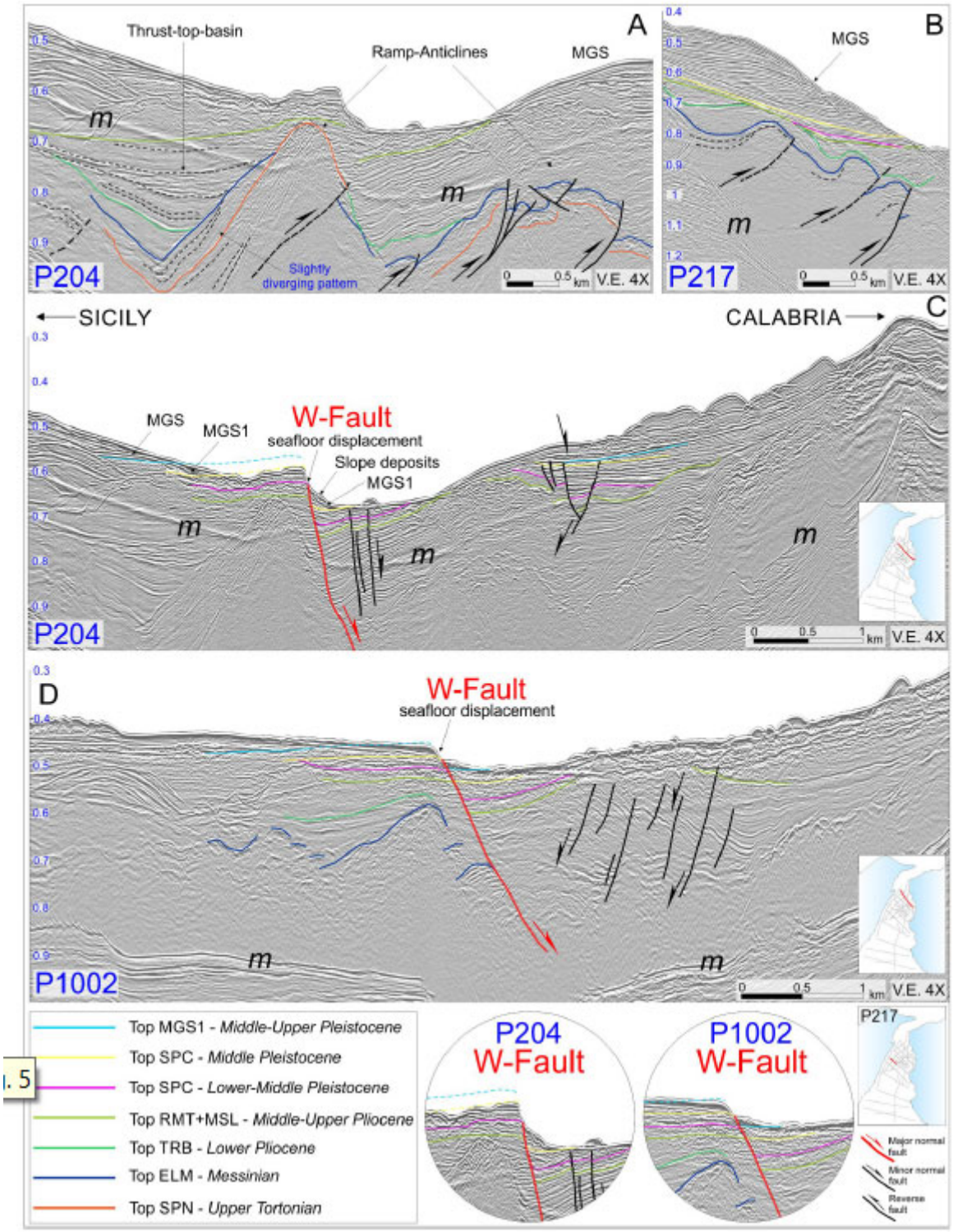
A
Thrust-top-basin
Ramp-Anticlines
MGS
m
P204
Slightly diverging pattern
V.E. 4X
B
MGS
P217
C
SICILY
CALABRIA
MGS
MGS1
W-Fault
seafloor displacement
Slope deposits
MGS1
D
W-Fault
seafloor displacement
P1002
Top MGS1 - Middle-Upper Pleistocene
Top SPC - Middle Pleistocene
Top SPC - Lower-Middle Pleistocene
Top RMT+MSL - Middle-Upper Pliocene
Top TRB - Lower Pliocene
Top ELM - Messinian
Top SPN - Upper Tortonian
P204 W-Fault
P1002 W-Fault
Major normal fault
Minor normal fault
Reverse fault

Figure 5

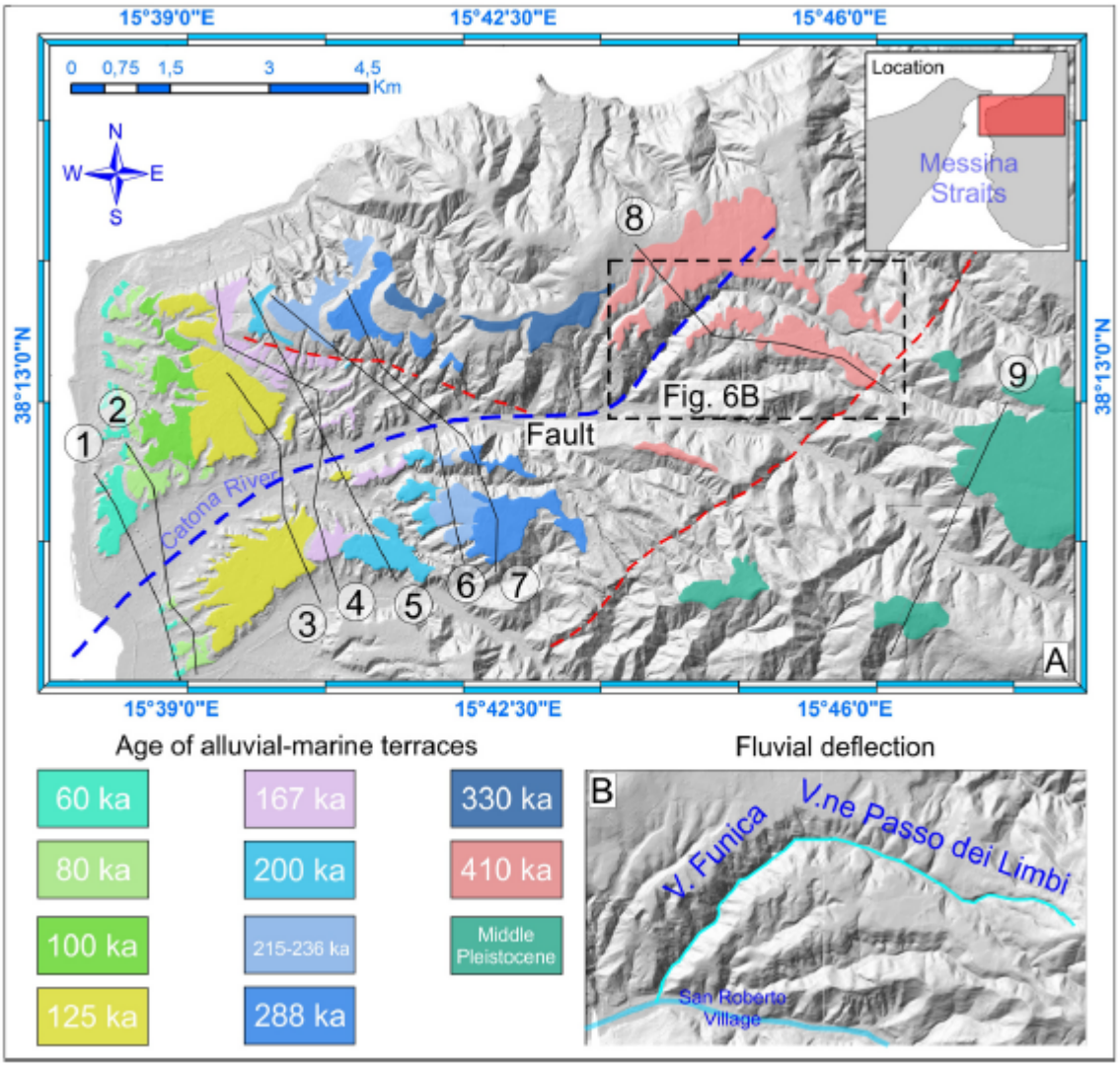
15°39'0"E
15°42'30"E
15°46'0"E
0 0,75 1,5 3 4,5 Km
N
W
E
S
Location
Messina Straits
38°13'0"N
8
9
Fig. 6B
Fault
1
2
Calona River
3
4
5
6
7
A
Age of alluvial-marine terraces
60 ka
80 ka
100 ka
125 ka
167 ka
200 ka
215-236 ka
288 ka
330 ka
410 ka
Middle Pleistocene
Fluvial deflection
B
V. Funica
V.ne Passo dei Limbi
San Roberto Village

Figure 6

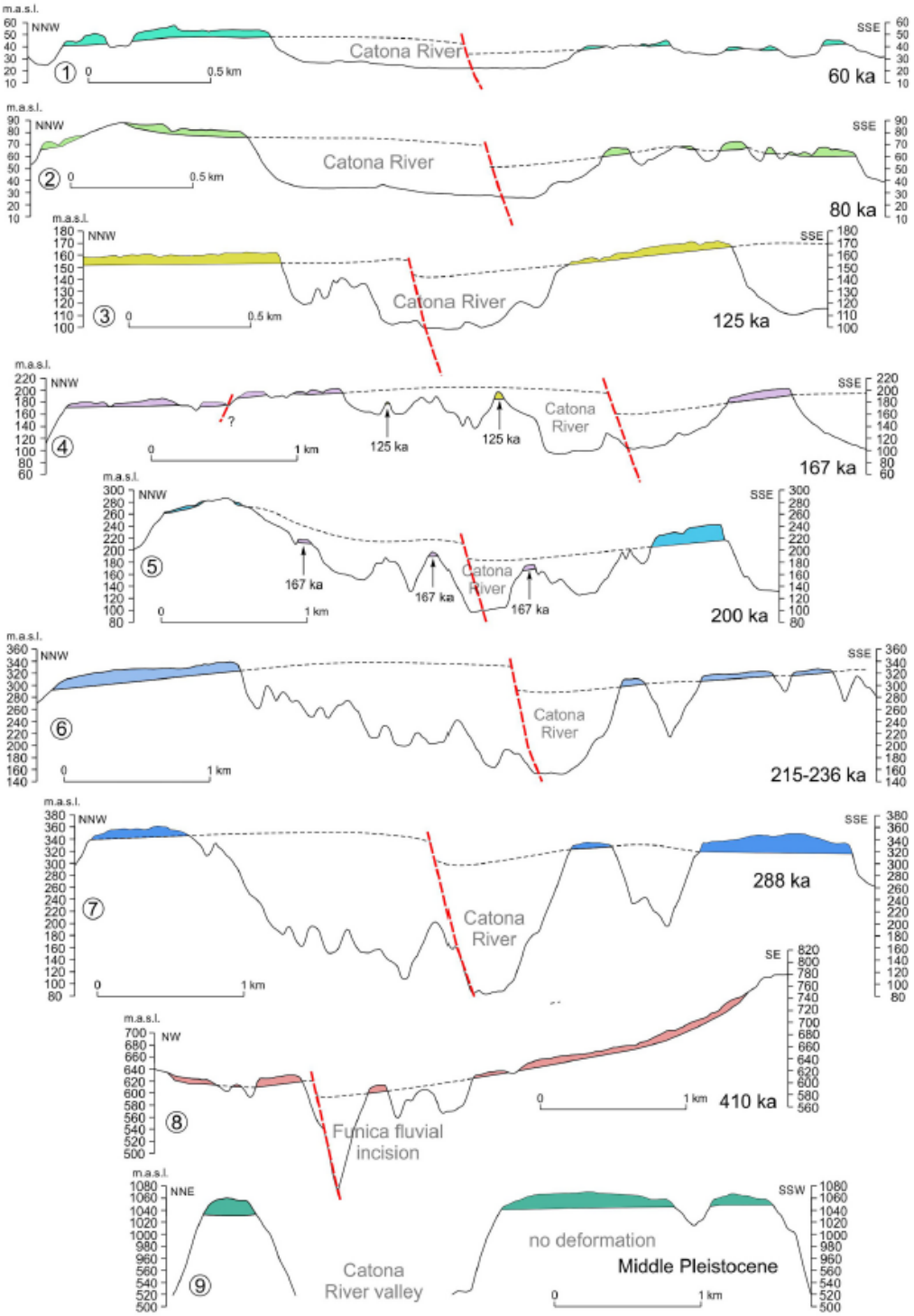
m.a.s.l.
NNW
SSE
Catona River
60 ka
80 ka
125 ka
167 ka
200 ka
215-236 ka
288 ka
410 ka
125 ka
167 ka
Fiumica fluvial incision
NW
SE
NNE
SSW
Catona River valley
no deformation
Middle Pleistocene
0
0.5 km
1 km

Figure 7

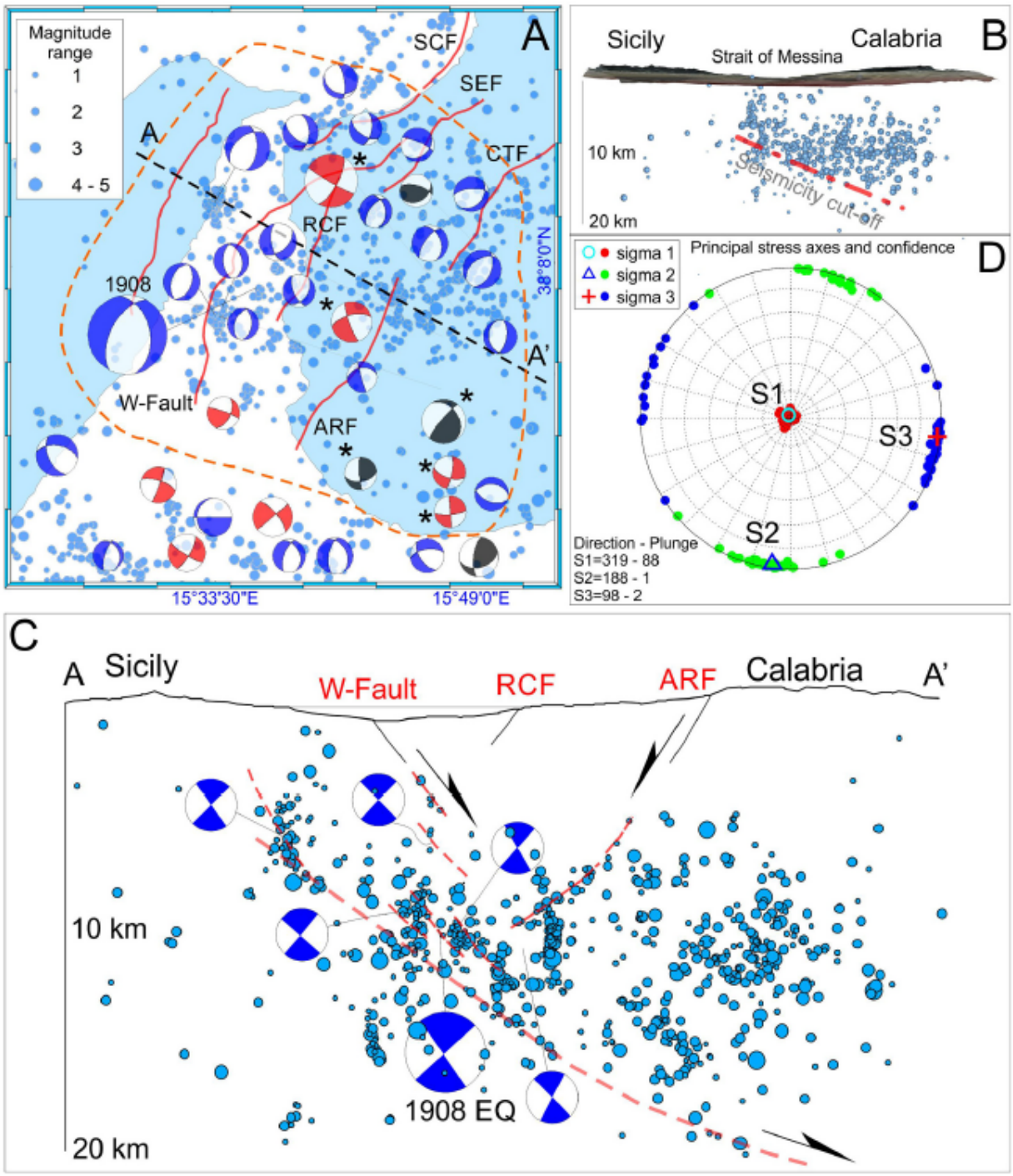
A
Magnitude range
1
2
3
4 - 5
SCF
SEF
CTF
RCF
ARF
W-Fault
1908
A
A'
38°80'N
15°33'30"E
15°49'0"E
B
Sicily
Calabria
Strait of Messina
10 km
20 km
Seismicity cut-off
D
Principal stress axes and confidence
sigma 1
sigma 2
sigma 3
S1
S2
S3
Direction - Plunge
S1=319 - 88
S2=188 - 1
S3=98 - 2
C
A
Sicily
W-Fault
RCF
ARF
Calabria
A'
10 km
20 km
1908 EQ

Figure 8

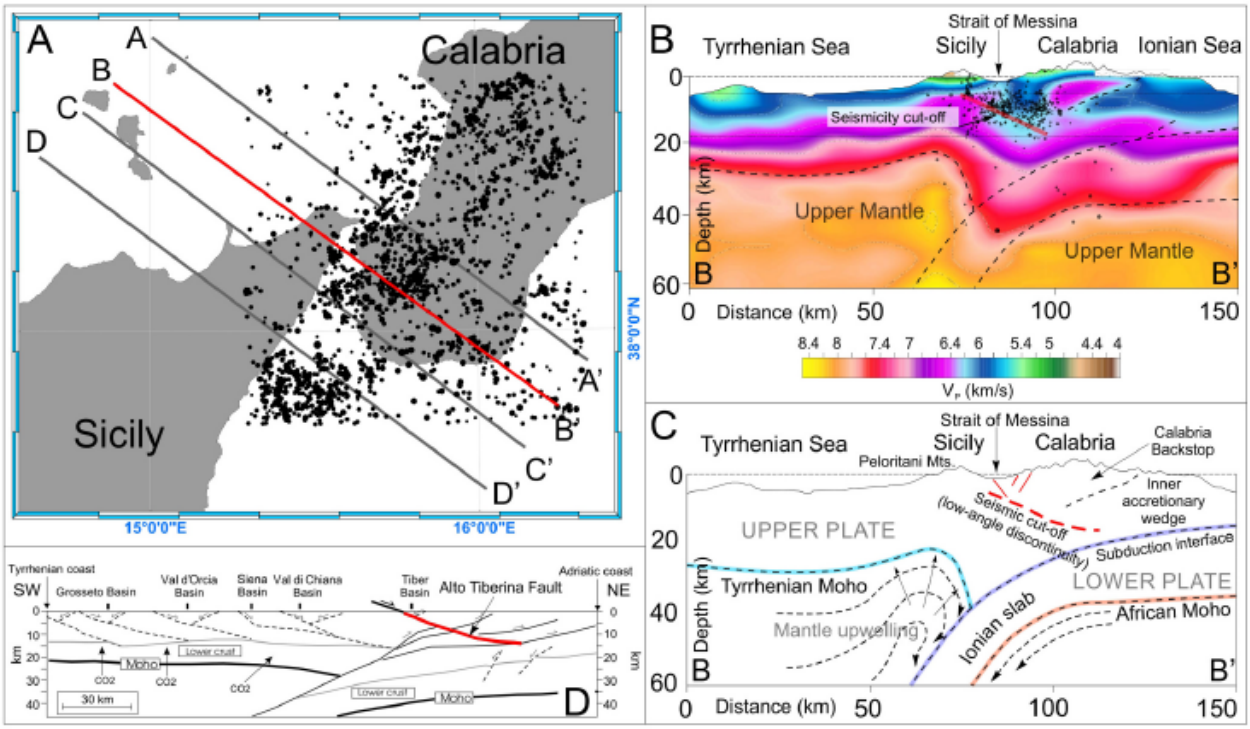
A
Calabria
Sicily
A
B
C
D
A'
B'
C'
D'
15°0'0"E
16°0'0"E
38°0'0"N
B
Tyrrhenian Sea
Strait of Messina
Sicily
Calabria
Ionian Sea
Seismicity cut-off
Upper Mantle
Upper Mantle
Depth (km)
Distance (km)
Vp (km/s)
C
Tyrrhenian Sea
Strait of Messina
Sicily
Calabria
Peloritani Mts
Calabria Backstop
Inner accretionary wedge
Seismic cut-off (low-angle discontinuity)
Subduction interface
UPPER PLATE
LOWER PLATE
Tyrrhenian Moho
Mantle upwelling
Ionian slab
African Moho
Tyrrhenian coast
SW
Grosseto Basin
Val d'Orcia Basin
Siena Basin
Val di Chiana Basin
Tiber Basin
Alto Tiberina Fault
Adriatic coast
NE
Moho
Lower crust
CO2
30 km
D

Figure 9

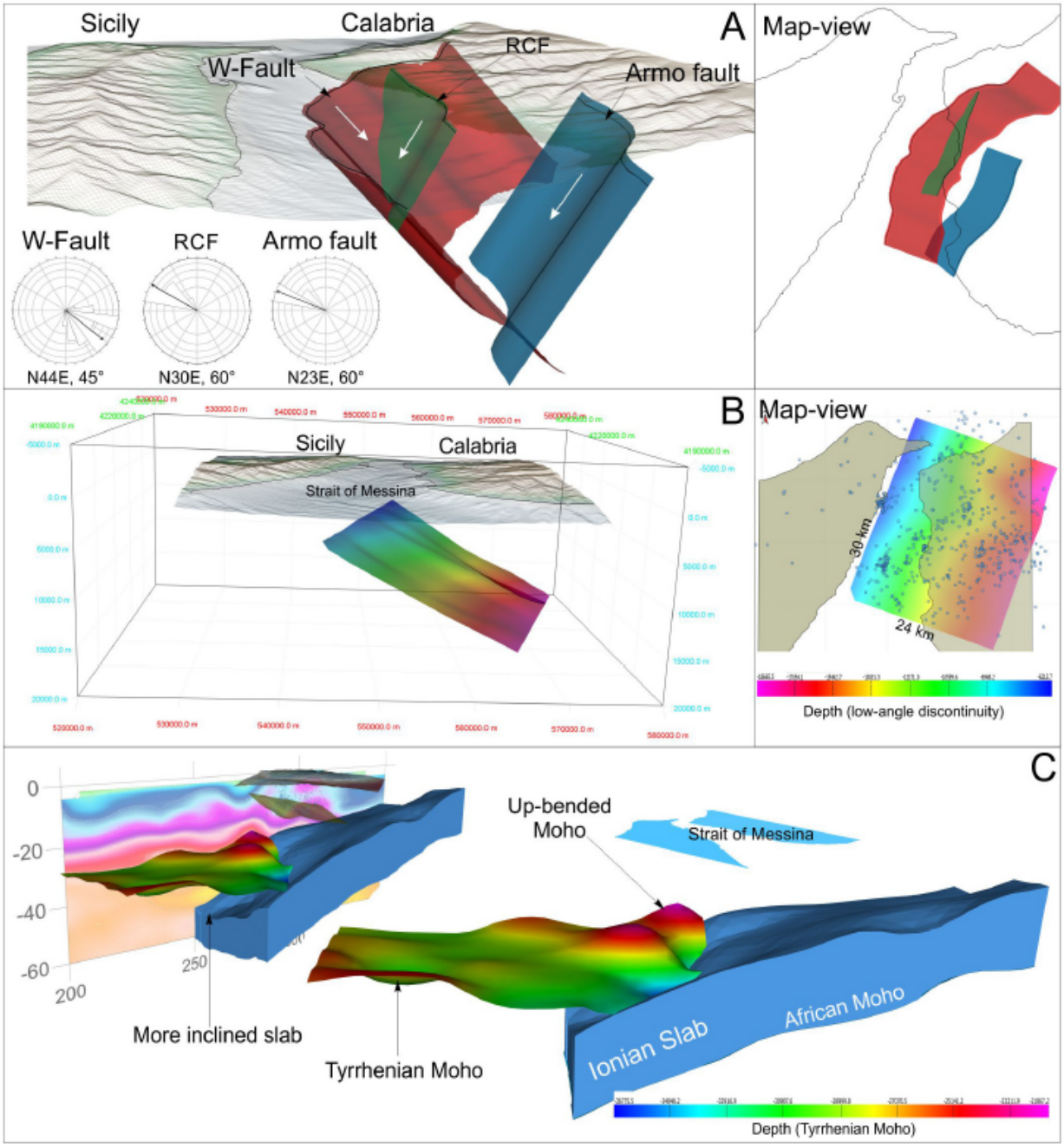
A
Sicily
Calabria
W-Fault
RCF
Armo fault
W-Fault
RCF
Armo fault
N44E, 45°
N30E, 60°
N23E, 60°
Map-view
B
Sicily
Calabria
Strait of Messina
Map-view
30 km
24 km
Depth (low-angle discontinuity)
C
0
-20
-40
-60
200
250
Up-bended
Moho
Strait of Messina
More inclined slab
Tyrrhenian Moho
Ionian Slab
African Moho
Depth (Tyrrhenian Moho)

Figure 10

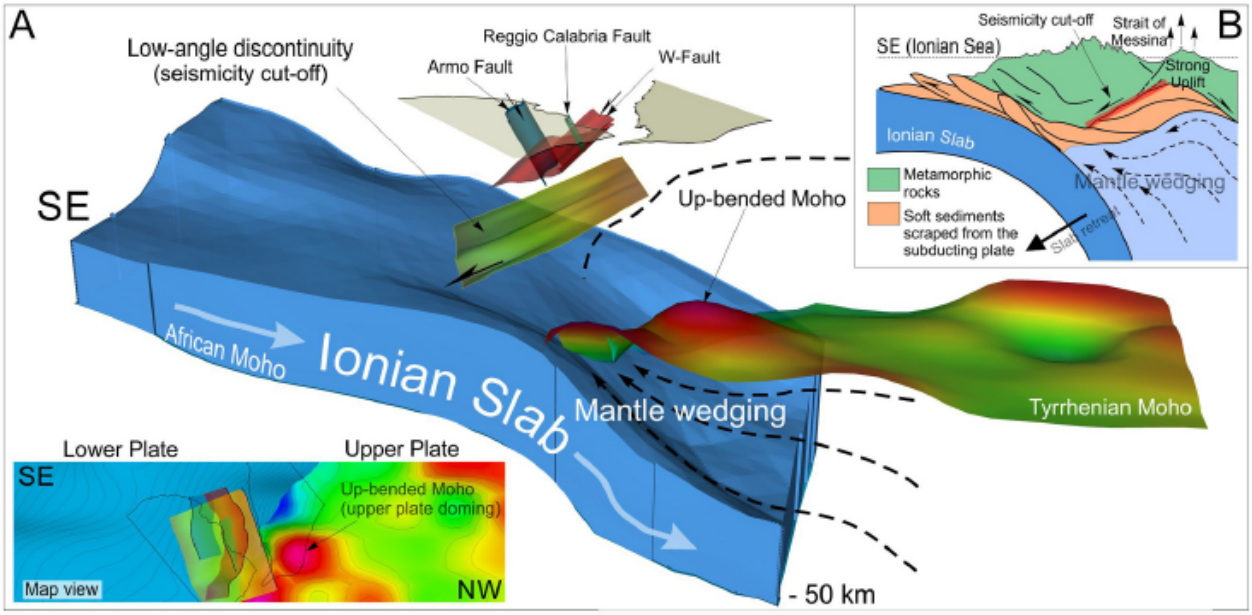
A
Low-angle discontinuity
(seismicity cut-off)
Reggio Calabria Fault
Armo Fault
W-Fault
SE
Up-bended Moho
African Moho
Ionian Slab
Mantle wedging
Tyrrhenian Moho
Lower Plate
Upper Plate
SE
Up-bended Moho
(upper plate doming)
Map view
NW
- 50 km
B
Seismicity cut-off
Strait of
Messina
SE (Ionian Sea)
Strong
Uplift
Ionian Slab
Metamorphic
rocks
Soft sediments
scraped from the
subducting plate
Mantle wedging
Slab retreat

Figure 11

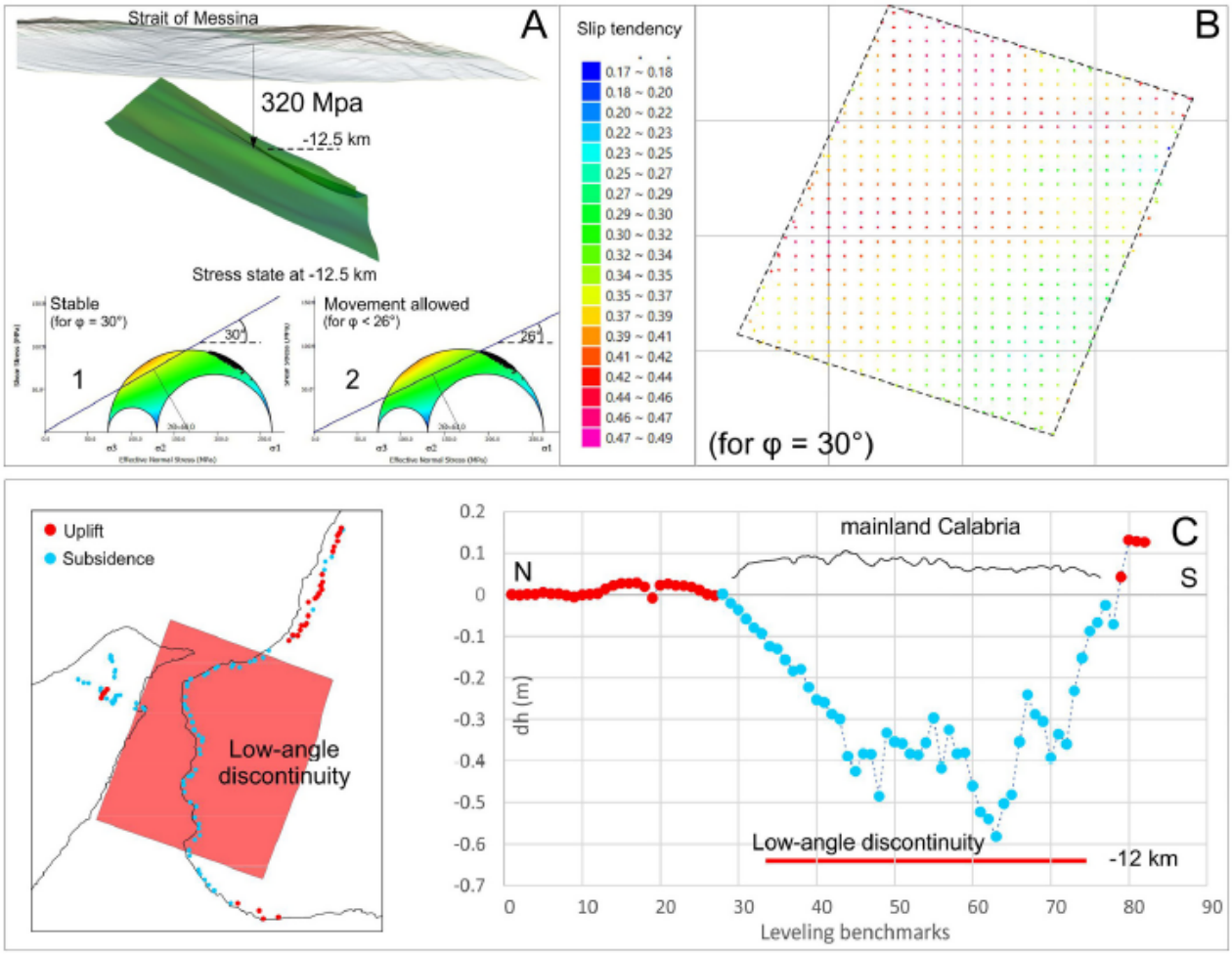
Strait of Messina
A
320 Mpa
-12.5 km
Stress state at -12.5 km
Stable
(for φ = 30°)
30°
1
Movement allowed
(for φ < 26°)
26°
2
Slip tendency
0.17 ~ 0.18
0.18 ~ 0.20
0.20 ~ 0.22
0.22 ~ 0.23
0.23 ~ 0.25
0.25 ~ 0.27
0.27 ~ 0.29
0.29 ~ 0.30
0.30 ~ 0.32
0.32 ~ 0.34
0.34 ~ 0.35
0.35 ~ 0.37
0.37 ~ 0.39
0.39 ~ 0.41
0.41 ~ 0.42
0.42 ~ 0.44
0.44 ~ 0.46
0.46 ~ 0.47
0.47 ~ 0.49
B
(for φ = 30°)
Uplift
Subsidence
Low-angle discontinuity
mainland Calabria
C
N
S
dh (m)
0.2
0.1
0
-0.1
-0.2
-0.3
-0.4
-0.5
-0.6
-0.7
Low-angle discontinuity
-12 km
0
10
20
30
40
50
60
70
80
90
Leveling benchmarks

Figure 12

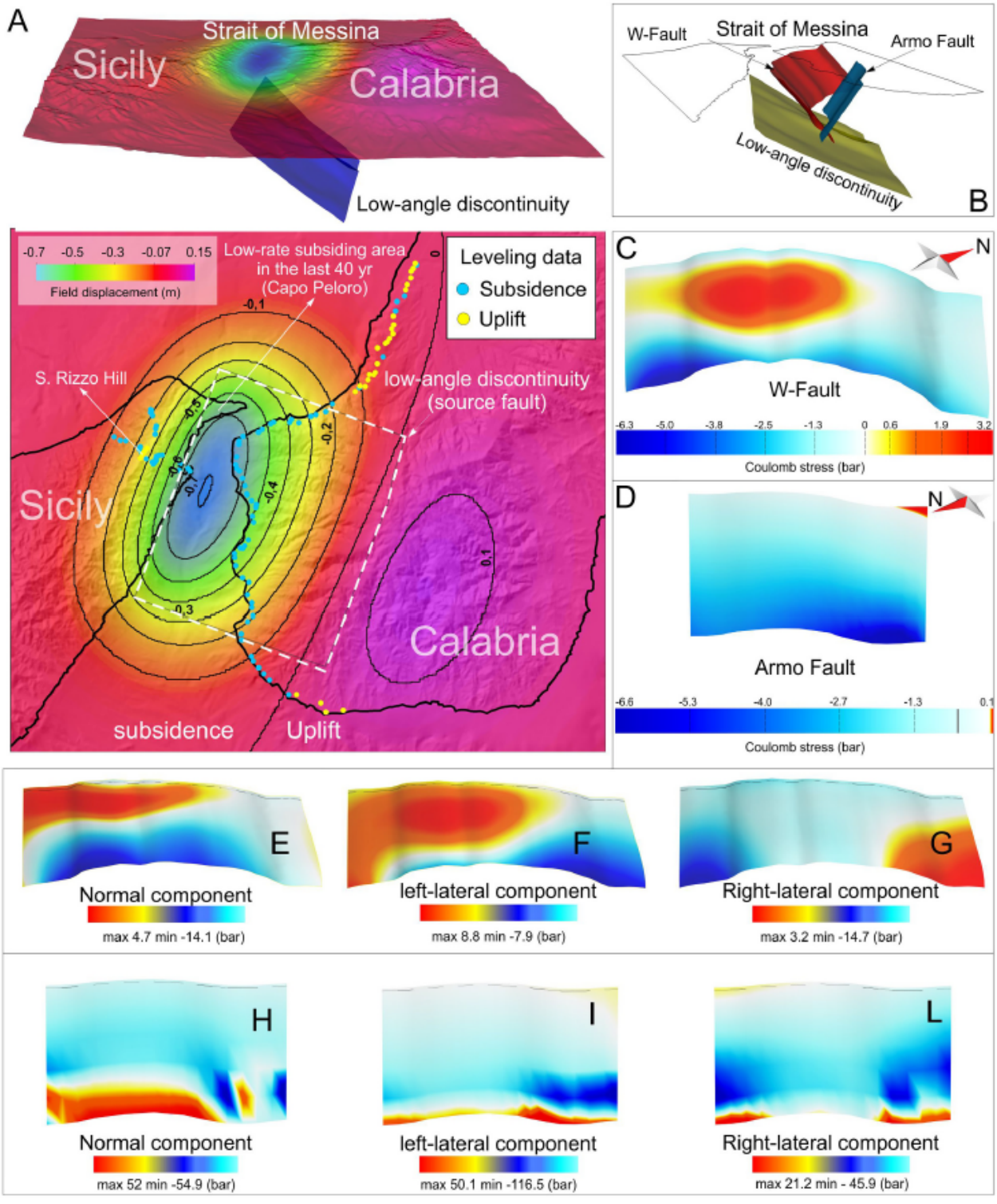
A
Strait of Messina
Sicily
Calabria
Low-angle discontinuity
W-Fault
Strait of Messina
Armo Fault
Low-angle discontinuity
B
-0.7 -0.5 -0.3 -0.07 0.15
Field displacement (m)
Low-rate subsiding area
in the last 40 yr
(Capo Peloro)
Leveling data
Subsidence
Uplift
S. Rizzo Hill
low-angle discontinuity
(source fault)
Sicily
Calabria
subsidence
Uplift
C
N
W-Fault
-6.3 -5.0 -3.8 -2.5 -1.3 0 0.6 1.9 3.2
Coulomb stress (bar)
D
N
Armo Fault
-6.6 -5.3 -4.0 -2.7 -1.3
Coulomb stress (bar)
E
Normal component
max 4.7 min -14.1 (bar)
F
left-lateral component
max 8.8 min -7.9 (bar)
G
Right-lateral component
max 3.2 min -14.7 (bar)
H
Normal component
max 52 min -54.9 (bar)
I
left-lateral component
max 50.1 min -116.5 (bar)
L
Right-lateral component
max 21.2 min - 45.9 (bar)

Figure 13

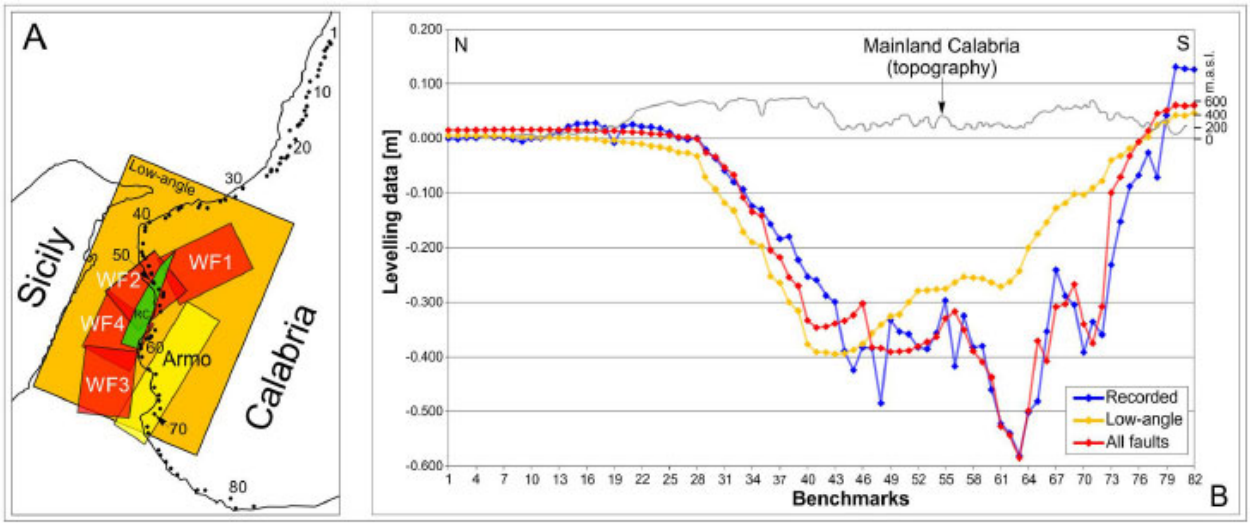
A
Sicily
Calabria
Low-angle
WF1
WF2
WF3
WF4
Armo
1
10
20
30
40
50
60
70
80
B
N
S
Mainland Calabria
(topography)
m.a.s.l.
600
400
200
0
Levelling data [m]
0.200
0.100
0.000
-0.100
-0.200
-0.300
-0.400
-0.500
-0.600
1 4 7 10 13 16 19 22 25 28 31 34 37 40 43 46 49 52 55 58 61 64 67 70 73 76 79 82
Benchmarks
Recorded
Low-angle
All faults

Figure 14

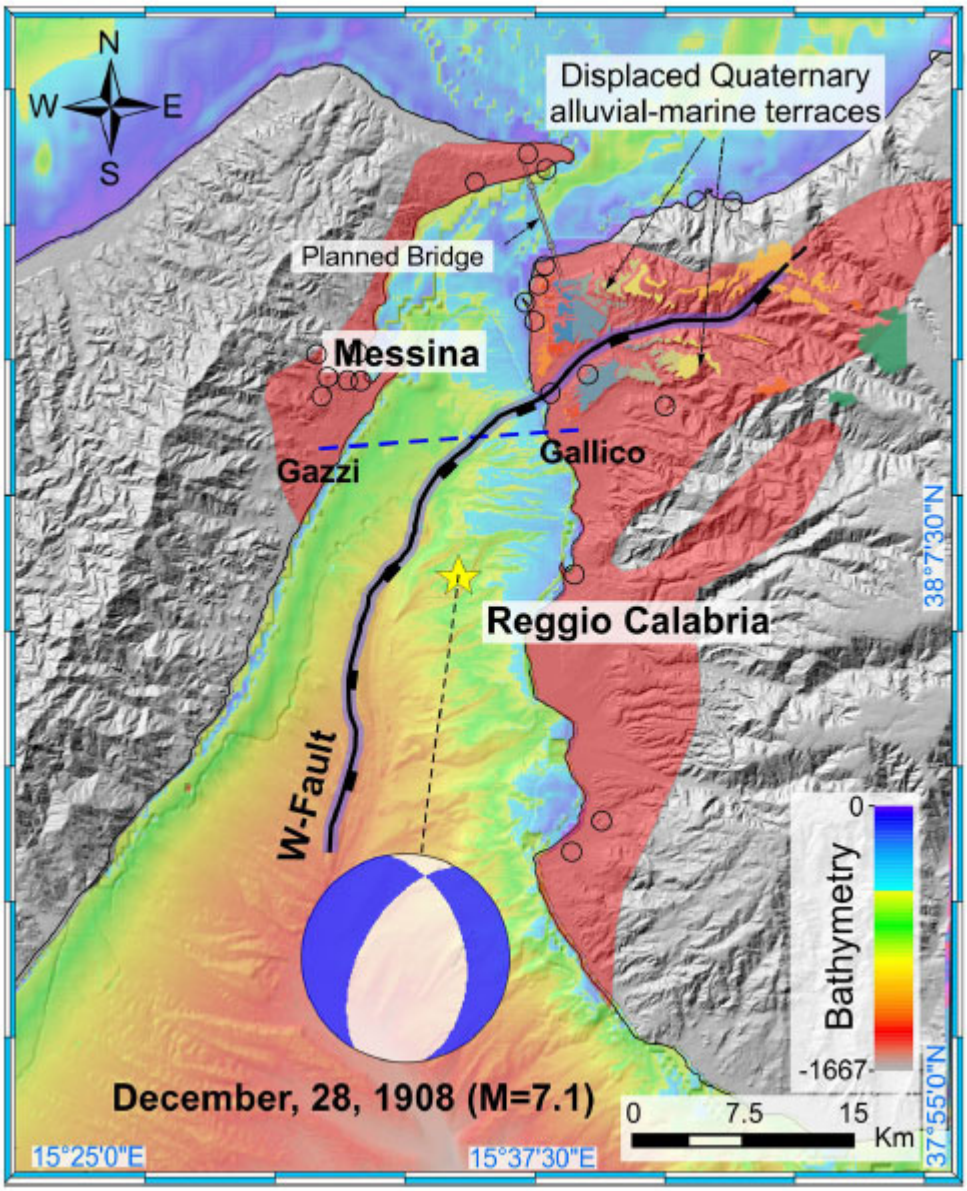
N
W
E
S
Displaced Quaternary
alluvial-marine terraces
Planned Bridge
Messina
Gallico
Gazzi
Reggio Calabria
W-Fault
Bathymetry
0
-1667
December, 28, 1908 (M=7.1)
0
7.5
15
Km
15°25'0"E
15°37'30"E
38°7'30"N
37°55'0"N

Figure 15

1694

1695

Table 1
Model parameters and related uncertainties resulting from levelling data inversion. Normal and left-lateral dislocation components are positive. The depth of the sources is referred to the sea level.

Fault parameters	Low-angle discontinuity	Armo fault	Reggio Calabria fault	W-fault segment 1	W-fault segment 2	W-fault segment 3	W-fault segment 4
x (m)	548468 (fixed)	560785 (fixed)	557625 (fixed)	562180 (fixed)	554283 (fixed)	548322 (fixed)	549962 (fixed)
y (m)	4225731 (fixed)	4211933 (fixed)	4221901 (fixed)	4229344 (fixed)	4225621 (fixed)	4212327 (fixed)	4219754 (fixed)
z (m)	−6213 (fixed)	0 (fixed)	0 (fixed)	0 (fixed)	0 (fixed)	0 (fixed)	0 (fixed)
Length (km)	31.0 (fixed)	17.7 (fixed)	13.0 (fixed)	10.2 (fixed)	7.9 (fixed)	8.4 (fixed)	7.7 (fixed)
Width (km)	24.0 (fixed)	9.0 (fixed)	9.0 (fixed)	9.0 (fixed)	9.0 (fixed)	9.0 (fixed)	9.0 (fixed)
Azimuth (°)	N23E (fixed)	N31E (fixed)	N20E (fixed)	N64E (fixed)	N50E (fixed)	N7E (fixed)	N25E (fixed)
Dip-angle (°)	24.32 (fixed)	60.0 (fixed)	60.0 (fixed)	45.0 (fixed)	45.0 (fixed)	45.0 (fixed)	45.0 (fixed)
Strike-slip (m)	0.0 (fixed)	0.00 ± 0.00	0.00 ± 0.00	2.17 ± 0.01	2.30 ± 0.00	2.3 ± 0.00	1.40 ± 0.01
Dip-slip (m)	1.13 ± 0.01	0.03 ± 0.01	0.00 ± 0.00	0.21 ± 0.01	0.18 ± 0.01	4.46 ± 0.01	0.00 ± 0.00

1696

1697 Tab 1